IEEE Access
Multidisciplinary ⋮ Rapid Review ⋮ Open Access Journal

Received 9 January 2024, accepted 5 March 2024, date of publication 11 March 2024, date of current version 18 March 2024.

Digital Object Identifier 10.1109/ACCESS.2024.3375399

RESEARCH ARTICLE

Intensification of Electric Field Stresses in Field Aged 380-kV Composite Insulators Due to Loss of Hydrophobicity

MANSOOR ASIF[1,2], KHALED AL-SOUFI[1], UMER AMIR KHAN[2,3], AND LUAI M. ALHEMS[1]

[1]Applied Research Center for Metrology, Standards and Testing (ARC-MST), Research and Innovation, KFUPM, Dhahran 31261, Saudi Arabia
[2]Electrical Engineering Department, College of Engineering and Physics, KFUPM, Dhahran 31261, Saudi Arabia
[3]Interdisciplinary Research Center for Sustainable Energy Systems, Research and Innovation, KFUPM, Dhahran 31261, Saudi Arabia

Corresponding author: Umer Amir Khan (umeramir.khan@kfupm.edu.sa)

This work was supported by the King Fahd University of Petroleum and Minerals (KFUPM).

ABSTRACT Polymer based composite high voltage insulators (HVIs) due to their hydrophobic surfaces have consistently outperformed the traditional ceramic insulators in highly contaminating coastal-desert environments. However, the harsh environment causes polymer surfaces of these HVIs undergo rapid ageing leading to permanent loss of hydrophobicity. In this paper, we have presented three samples of 380 kV composite HVIs with a service life of over ten years near west coast of the Kingdom of Saudi Arabia. Material investigation using scanning electron microscopy (SEM) and energy-dispersive X-ray spectroscopy revealed substantial surface deterioration and change in the composition. Hydrophobicity investigations revealed that surface of the HVIs have become hydrophilic leading to accumulation of continuous films of water. Electrical withstand strength was evaluated using steam fog test showing significant decrease from the rated values. The distribution of electric field around an insulator is a key design criterion for HVIs. The consequences of loss of hydrophobicity on the electric field distribution across insulator surface is explained analytically and through numerical simulations based on Finite Element Method (FEM). The pristine and field aged HVIs are modelled and were covered with realistic water distributions observed during hydrophobicity tests. It has been observed that the intensity of electric field on field aged insulator surpasses the corona inception threshold at certain areas of the insulator, resulting in the initiation of corona discharge on the insulator's surface. This corona inception further causes surface deterioration and accelerated ageing in composite HVI.

INDEX TERMS Aging, composite insulators, electric field, finite element modeling, hydrophobicity.

I. INTRODUCTION

The electrical power infrastructure of any country is one of its most vital assets, demanding consistent functionality and operational resilience throughout the year. Transmission line faults can disrupt electrical power over large scale and can result in huge losses for national economy. Therefore, it is extremely crucial for power system operators to ensure that the power system remains free of faults [1], [2], [3]. Transmission line faults can result in large scale blackouts; therefore, it is crucial to proactively anticipate potential issues within transmission lines and promptly address them [4], [5].

Insulators in overhead lines are one of the most vulnerable parts of electrical power transmission, their breakdown can result in immediate shutdown of the transmission line. Power flow is impossible without insulation. Transmission systems are designed to utilize naturally occurring air as the major dielectric during power transmission. However, the solid insulation is also required at numerous points. Overhead transmission lines (OHTL) have insulators on every tower which allow the live conductors to hang from the towers while remain electrically isolated from the grounded metallic towers [6]. Hundreds of kilometers of OHTL can only operate as long as each and every one out of thousands of insulators maintains their dielectric strength. As soon as an insulator will lose its strength, the whole power through the OHTL

The associate editor coordinating the review of this manuscript and approving it for publication was Su Yan.

will be disrupted. Therefore, the health assessment of field insulators is one of the most important aspect in successful operation of power systems [7], [8], [9], [10], [11], [12], [13], [14], [15], [16], [17].

High voltage OHTL has HV insulators (HVI) which are classified into two major types namely ceramic and composite insulators. Ceramic HVI are the oldest and the most rugged types of insulators which can perform for decades in the field without being affected by weather cycles, solar ultraviolet rays, and material deterioration. However, they have fundamental weaknesses which have led to adoption of composite HVI by many transmission system operators (TSOs) across the globe. Ceramic HVIs are extremely heavy, brittle, and expensive in terms of transportation and tower size. One of the most detrimental weakness of ceramic HVI is that they are hydrophilic in nature. They attract water deposition on their surface which when mixed with pollutant salts, drastically decrease their creepage resistance and result in flashover. They do not pose high risk in areas where there is regular rainfall or clear air conditions, but they are a recipe of disaster in coastal, desert, and industrial regions where environmental contamination is very challenging. If the region is composed of both desert and coastal areas, like the coasts of Saudi Arabia, these insulators experience frequent flashover faults [18], [19], [20], [21], [22], [23], [24], [25], [26], [27], [28], [29], [30].

Composite HVI are light weight, easy to handle, less costly and possess the fundamental property of hydrophobicity which makes them ideal to be installed in terrains with high rate of contamination, like coastal and desert regions [31], [32], [33]. The hydrophobic surface of composite HVIs, resist development of conductive paths on the surface and hence prevent flashover at high voltages in coastal and desert regions [34], [35]. However, the fundamental drawback associated with them is that they are prone to deterioration and damage in harsh environment under the influence of electrical and mechanical stress in addition to UV radiations, chemical reactions, thermal processes and water ingress.

The effective field life of composite HVI is still a debatable topic and there is no specific answer [36], [37], [38]. It varies from few years to well over a decade in the field. It is imperative to study the effects of loss of hydrophobicity on the performance of insulators in the field and it is the objective of the proposed research work [39], [40], [41], [42], [43], [44], [45], [46], [47].

In this research work we have investigated the effects of loss of hydrophobicity due to field ageing in composite HVIs and their consequent effect on their ability to withstand high voltages of OHTL under severe environmental conditions. The composite HVI after having a considerable service life in the field consisting of coastal-desert region of Saudia Arabia has been selected for this research work. The composite HVIs had a service life of ten years and have been exposed to UVR, severe heat cycles, sandstorms, and other environmental effects. The following aspects are covered in this research paper:

1) The physical ageing effects on the composite material of field insulators are identified. This includes visual inspection, Scanning Electron Microscopy (SEM) to evaluate the surface deterioration, and Energy-Dispersive X-ray Spectroscopy (EDX) for determining the chemical composition.
2) Electrical test approach of IEC 60507 were adapted to make them suitable for assessment of withstand strength of the field aged insulators [48].
3) The loss of hydrophobicity is investigated by performing hydrophobicity tests for the field-aged insulators and comparing with pristine insulators made of same material and the manufacturer. These tests were performed according to IEC62073 and hydrophobicity class for both types of insulators was identified [49].
4) The effects of waterdrops deposited on insulator surface upon electric field distribution across the insulator is studied by conducting simulations in COMSOL Multiphysics. Moreover, the shape and size of waterdrops which represent the hydrophobicity class are also simulated to analyze their effects on intensification of electrical field around them.
5) Lastly, the field insulators with poor hydrophobicity is modelled in COMSOL and the electric field distribution along the insulator is analyzed and compared with highly hydrophobic pristine insulator. Considerable field intensification along the composite HVI surface was observed which will consequently result in decrease in dielectric strength and increase the chances of flashover across the composite insulator.

This research paper is structured as follows. Section II presents an analysis of the Field Aged samples based on various investigations. Section III presents the effects of waterdrops on electric field distribution across an insulator surface and Section IV presents the modeling of field insulators in COMSOL with poor hydrophobicity levels and studies the effects of deformed and large waterdrops on dielectric stress. The presented work will act as resource for both the academic researchers and manufacturers about the performance of composite HVI in the field for extended periods of time.

II. FIELD AGED SAMPLES OF COMPOSITE INSULATORS

Numerous samples of field aged HVIs were received at High Voltage Testing Laboratory located in King Fahd University of Petroleum for detailed investigations and analysis. Three samples were selected for detailed analysis as explained in the following sections.

A. ENVIRONMENTAL STRESSES SUBJECTED TO FIELD INSULATORS

The HVI installed in high voltage OHTL are subjected to severe environmental conditions throughout the years. The degradation in composite insulators due to environmental effects cannot be emulated in labs. To understand the

effects of loss of hydrophobicity on composite HVI, the best-scenario is availability of field insulators which have performed in the field and have been subjected to various types of environmental stresses including UVR, weather cycles, and sandstorms. The coastal regions in Saudi Arabia offers one of the toughest environments for composite insulators to operate. The weather is extremely hot with very scarce rainfall and composite insulators located in desert coastal regions show drastic ageing effects [50], [51].

Fig. 1 shows a typical 380 kV tower located in the transmission lines on western coastal region of Saudi Arabia. The OHTL is a double circuit line. Each phase of the line is held by two composite insulators and single tower contains twelve composite insulators. The OHTL is exposed to environmental condition for decades. The insulators are exposed to UVR and thermal radiations from the sun, seasonal and daily temperature cycles, sandstorms, deposit of environmental contaminants including coastal sand and industrial flue gases. Insulators are expected to face all these conditions without dereasing the reliability of the power system in general and OHTL in particular.

Fig. 2 lists down the typical stresses that the HVI insulator is subjected to. It should be noted that the insulator is expected to withstand these stresses for decades of its operational life. Electrical stresses are caused by the quasi electrostatic field that exists due to high voltage transmission line. Occasionally, this stress can increase momentarily on the insulators during switching or lightning impulses. Partial discharges start to appear in insulators as they age and the dielectric strength decreases due to electrical stress on the insulators.

The mechanical stresses that the HVI is subjected to be severe during hail storms due to swinging power lines. The thermal stresses can be diurnal and also seasonal. The temperatures in deserts can fall down to a considerable amount during night times. Also, the high temperature-humidity regimes in Saudi Arabia can result in extreme thermal stress on insulators.

The fast blowing north wind in Saudi Arabia, also referred to as Shamal, can give rise to severe dust storms. These desert sand can be detrimental to insulator surfaces. Also, the industrial pollutants in the air react with polymer surface under high temperature and humid conditions. In addition, the costal regions of the Arabian peninsula have high atmospheric chloride levels in coastal regions.

The coastal regions of Saudi Arabia experience few cloudy days throughout the year, therefore insulators are exposed to high level of UV radiations throughout the year. Particularly high energy UV-B radiations are potent enough to cause photo-oxidation and scission of molecular bonds. The C-Si and C-H bonds on silicone rubber surface can break and form free radicals [52]. These free radicals have high energy and are prone to cross-linking reaction as well as reaction with atmospheric oxygen to form hydrophilic OH groups on the polymer surface [53]. The surface composition starts to change under constant UV attack and hydrophobicity begins to decrease. The depolymerization and surface damage is much more significant at the surface than at the greater depths as depicted in Fig. 3 [54].

TABLE 1. Specifications of 380 kV Silicone Rubber Insulator.

Property	Value
Voltage Level	380 kV
Total Length	4910.52 mm
Arc Length	4552 mm
Creepage Distance	15458 mm
Specific Creepage Distance	41 mm/kV
Total Sheds	92
Small Sheds	47
Large Sheds	45
Insulation Material	Silicon Rubber
Support Rod	Fiber Glass
Electrodes with Corona Ring	Forged Steel
Specified Mechanical Load	160.1 kN
Corona Ring (tower)	8” (split)
Corona Ring (conductor)	12” (split)
60 Hz Dry Flashover	1524 kV
60 Hz Wet Flashover	1228 kV

B. PHYSICAL INSPECTION

Fig. 4 shows the dimensions and shape of a typical Silicone Rubber (SiR) composite HVIs installed in 380 kV OHTL in Saudi Arabia. The insulator is made up of Silicone Rubber (SiR) insulation material with support rod made up of glass fibre. The total length of the insulator is 4910.52 mm with an arc length of 4552 mm. The creepage distance is 15458 mm with specific creepage distance (SCD) of 41 mm/kV. The total number of sheds in the insulator are 92. Table 1 tabulates the specifications of the insulators collected from the field for further analysis.

Fig. 5 shows the insulators received from the field. The field aged HVI had a field service life of ten years. The insulators were carefully packed and sent to High Voltage Laboratory located in King Fahd University of Petroleum and Minerals for detailed investigations and analysis. Fig. 5 (a) shows deterioration of polymer coating on the shank and fiber glass was exposed in this region. Physical deformation of the sheds was observed as shed undulations as can be seen in Fig. 5 (b). Severe corrosion was observed on metallic parts including corona ring as shown in Fig. 5 (c). This is due to operation of OHTL in coastal region with highly saline environment. Chalking and whitening is also very evident in Fig. 5 along with deposits of contaminants including dust, sand, and soot as shown in in Fig. 5 (d).

C. MATERIAL INVESTIGATION

The superior insulation characteristics of SiR insulator is attributed to its hydrophobicity, which stems from low molecular weight (LMW) polymer chains at the surface of the insulator. During service, the contamination and moisture accumulation on the insulator surface can give rise to dry band arcing, resulting in the depolymerization of LMW polymer chains. The reduction in quantity of these polymer chains is represented by reduction in the Si/Al ratio. Additionally, aluminum trihydrate (ATH) is used as filler material in SiR

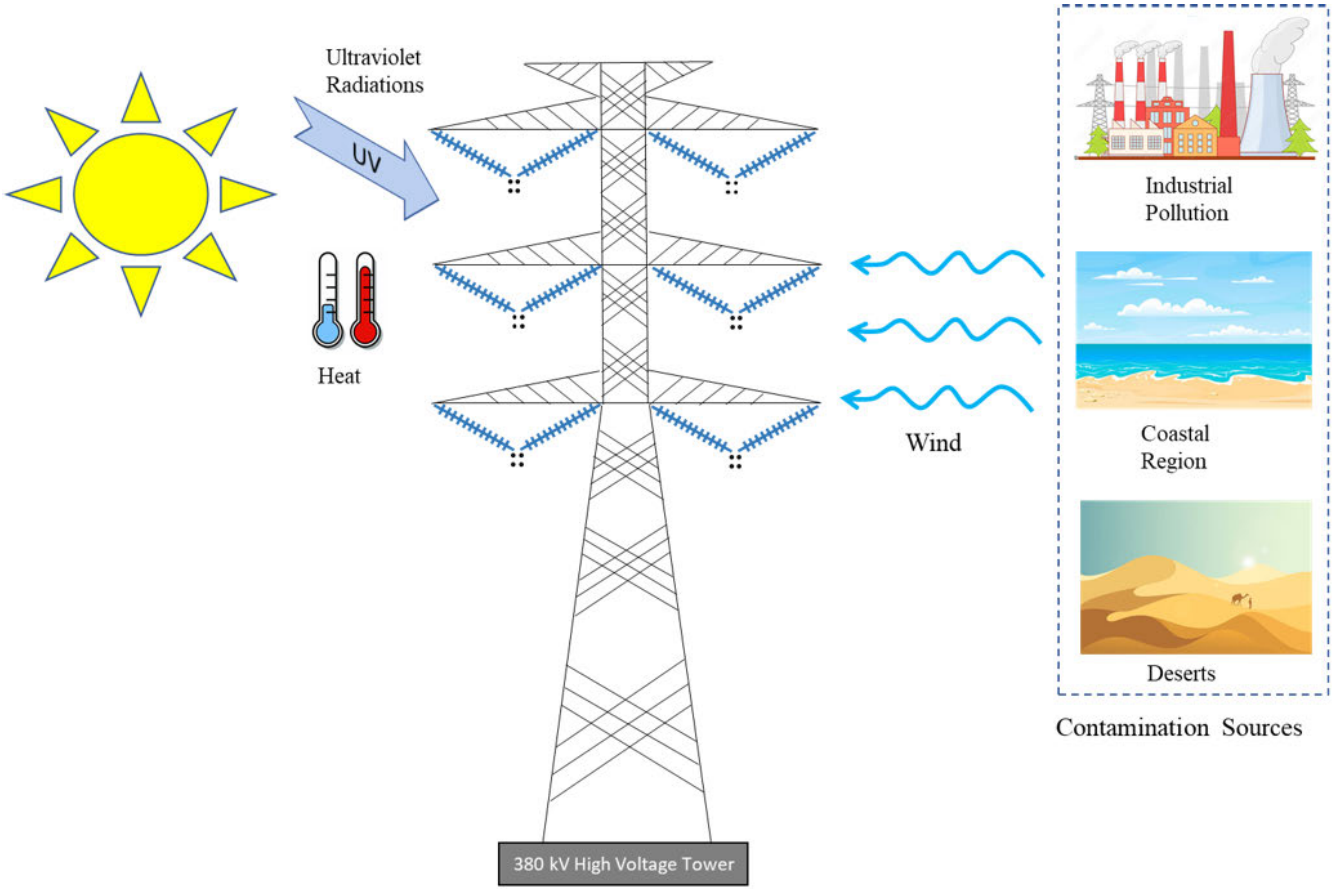

FIGURE 1. A typical 380 kV High Voltage Transmission Line tower located close to west coast of Saudi Arabia.The insulators on the tower are subjected to various environmental stresses throughout its life time.

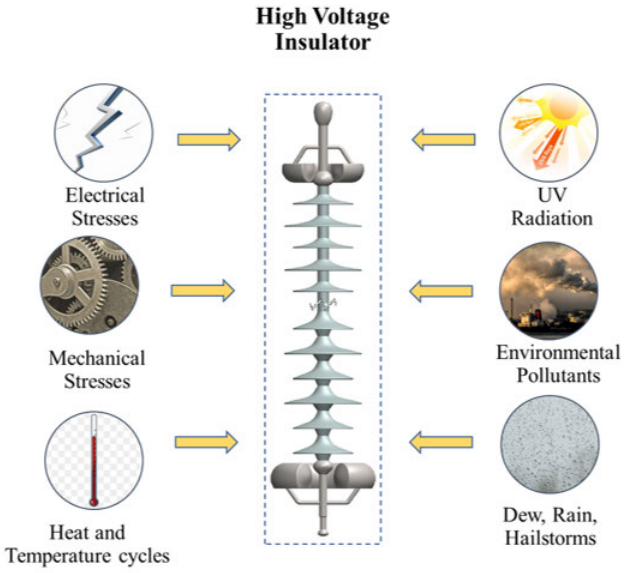

FIGURE 2. The stresses acting on High Voltage Insulators during their field life.

insulator to improve its tracking and erosion resistance. ATH filler in ageing insulator starts to cluster leading to loss of tracking and erosion resistance. As the top layer of SiR is eroded, dry band arcing commences in the next layer and hence the material continues to erode. This leads to a rough and hydrophilic surface of the insulator and reduced dielectric strength [55], [56].

To investigate the extent of damage caused to our field aged insulator by these well-known ageing processes, Scanning Electron Microscopy (SEM) and Energy Dispersive X-Ray spectroscopy (EDX) are performed. SEM gives an insight into the surface morphology, whereas EDX shows the chemical composition of aged insulator. Fig. 6 shows the results of these SEM and EDX analysis.

1) SCANNING ELECTRON MICROSCOPY ANALYSIS

Scanning electron microscopy (SEM), is performed by scanning an electron beam across the sample's surface. When these electrons interact with the sample, they produce various signals, including X-rays and secondary electrons. Secondary electrons originate from the top layers of the sample, providing a clear view of the surface. The contrast in these images is influenced by the sample's morphology. High-resolution imaging is possible in SEM due to the small diameter of the primary electron beam, offering valuable insights into surface conditions, such as insulator roughness.

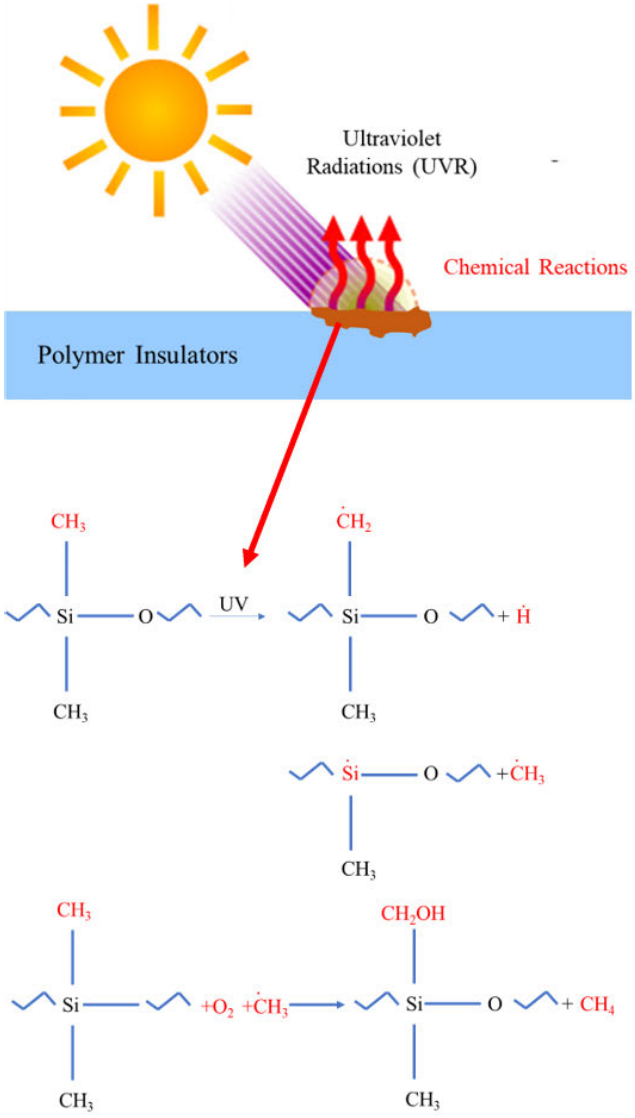

FIGURE 3. The detrimental effects of ultraviolet radiations coming from the sun. These radiations severely damage the top surface of HVI in the Field.

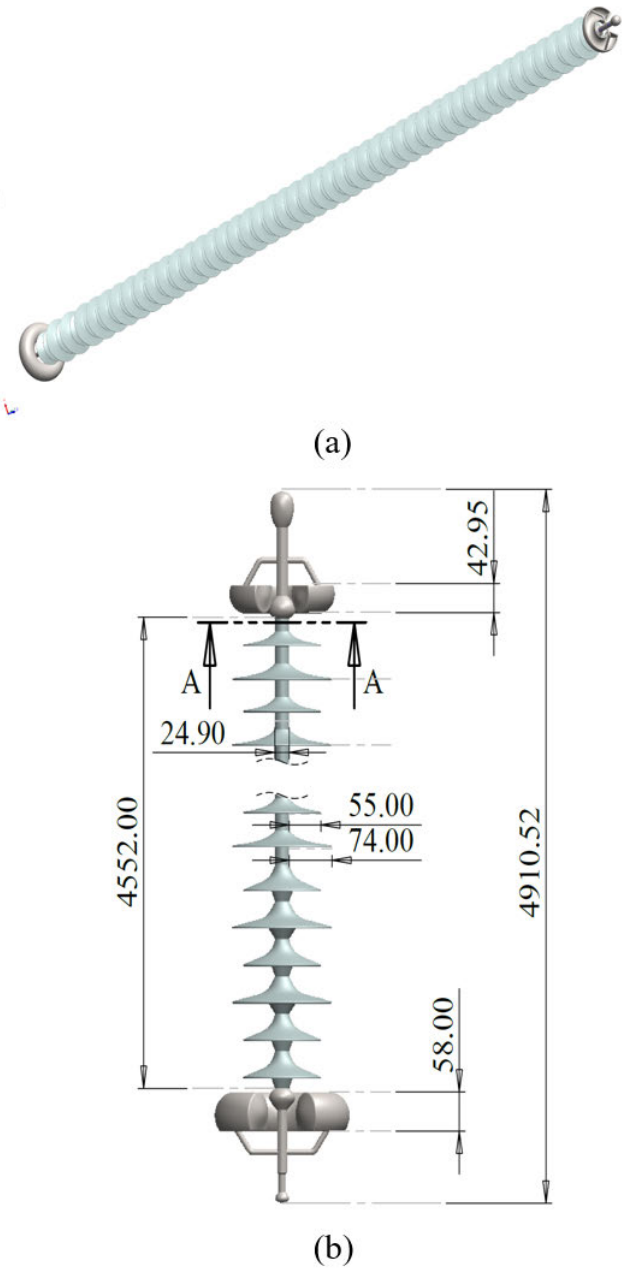

FIGURE 4. The shape and dimensions of a a Composite insulator used in 380 kV Overhead Transmission Lines.

Samples for SEM analysis were prepared by taking cutouts from sheds and shanks of both insulators. Selected micrographs at 100X representing shed and shank of the insulator are shown in Fig. 6 (a), (b), and (c). All the samples exhibit a coarse and rough surface morphology, indicating widespread surface damage. The SEM micrographs also reveal cracks and erosion, which results in large wetting angles, suggesting a potential loss of hydrophobicity. The cracks spread over the surface seem to act as capillaries, spreading the water over the surface and making the insulation hydrophilic.

2) ENERGY-DISPERSIVE X-RAY SPECTROSCOPY

EDX works by directing a focused electron beam onto the sample's surface. This interaction excites the sample's atoms, causing them to emit characteristic X-rays that are specific to the elements present. By detecting and quantifying these emitted X-rays, we can gain crucial insights into the elemental makeup of the SiR material, which is invaluable for assessing its aging process and overall performance.

The samples were thoroughly cleaned with water to remove atmospheric dust and other contaminants from the sample surface to ensure no interference with the results. Fig. 6 (d), (e) and (f) shows the result of EDX for field aged insulators. The EDX analysis was performed at different accelerating voltages ranging from 3 kV to 9 kV. The penetration of beam into the sample at 3 kV is the lowest and it increases with increasing voltage. Therefore, the 3 kV

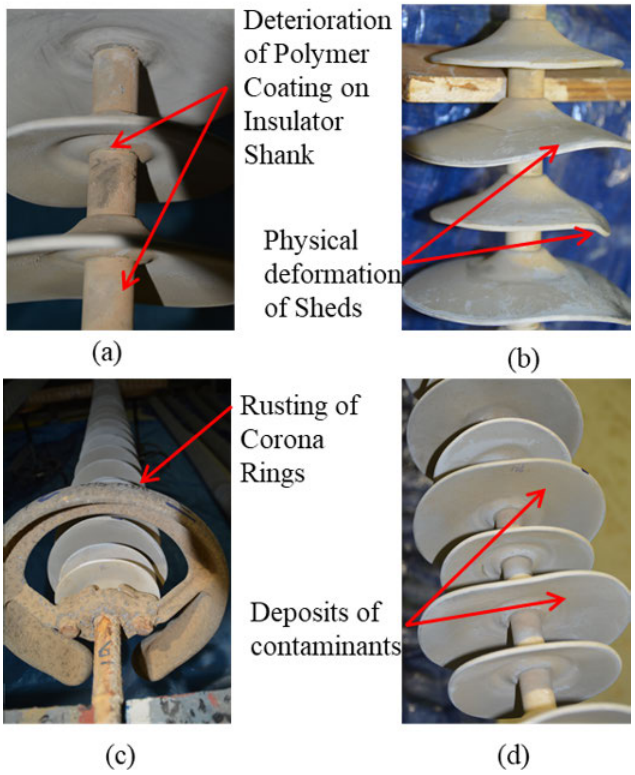

FIGURE 5. Visual Inspection of Field Aged Insulators.

beam, provides elemental information from the top layers of the surface. The Si/Al ratio obtained for a pristine insulator is very large indicating excellent hydrophobic properties. However, the Si/Al ratios obtained at 3 kV was low for both samples because LMW polymer chains rich in Si and present at the surface have been consumed due to degradation. Moreover, the Si/Al ratios show little variation through the entire range of accelerating voltages (3)-9 kV) used for all samples indicating an absence of protective Si-rich LMW chains in the bulk of the composite insulator. Lowered levels of Si/Al ratio are indicative of degradation which corroborates the evidence obtained by SEM imaging which showed rough surface.

Table 2 summarizes the result Si/Al ratios for pristine insulators and also three samples from field aged HVIs marked as FS01 to FS03. For different accelerating voltages, the Si:Al ratio of samples coming from the field has significantly decreased when compared with ratio for pristine insulators. This indicates the degradation of polymer surface and it will consequently change the surface properties of the insulator.

D. CONTAMINATION ASSESSMENT

Contamination was meticulously removed from selected areas of the insulators in accordance with IEC 60507 for evaluating the Equivalent Salt Deposit Density (ESDD) and Non-Soluble Deposit Density (NSDD) [48]. An equal number of small and large sheds, including the associated shanks, were chosen, each with an area of 1710.2 cm^2.

TABLE 2. EDX Analysis of SiR Samples Showing Si:Al Ratios at Different Accelerating Voltages.

Accelerating Voltage (kV)	Pristine	FS001	FS002	FS003
3	13.81	1.73	2.52	2.24
4	8.47	3.26	3.12	3,01
5	3.13	2.85	2.10	2.04
6	2.90	2.46	2.25	2.12
7	3.35	2.42	2.07	2.12
8	3.63	1.94	2.03	1.86
9	3.83	2.06	2.05	1.34

TABLE 3. Contamination Levels on Field Insulators.

Insulator Code	Sample Area (cm^2)	ESDD (mg/cm^2)	NSDD (mg/cm^2)
FS001	1710.2	0.19	0.88
FS002	1710.2	0.14	1.05
FS003	1710.2	0.17	0.99

For ESDD measurements, contaminants were removed from the sample area using clean cotton and then dissolved in 600 ml of distilled water. The resulting suspension was stirred for at least 2 minutes before measuring its volume conductivity and temperature. The salinity and resulting ESDD were then calculated following the procedure outlined in IEC 60507.

In the case of NSDD evaluation, contaminants were removed from the sample area using clean, oven-dried cotton with a known weight. Soluble deposits were subsequently flushed completely from the cotton using filter paper and distilled water. The cotton containing the non-soluble deposits was left behind, then dried in the oven again. The difference in weight between the clean, dried cotton and the cotton containing non-soluble deposits provides an indication of the quantity of non-soluble deposits, which is used to calculate NSDD.

The ESDD and NSDD measurements are reported in Table 3. It is important to note that the surface chalking also contributed to the relatively high value of NSDD.

E. ELECTRICAL INVESTIGATION

Through visual, SEM, and EDX investigations, it was evident that the composite insulator material has suffered considerable degradation. To investigate the effects of this degradation on the dielectric strength of the insulators, electrical withstand test was performed on three insulators received from the field. HVIs are most vulnerable to flashover in high humidity conditions, therefore, to replicate the field environment, flashover testing was performed in presence of steam fog inside the fog chamber. These tests were further compared with the specifications provided by the manufacturer for the withstand strength of new insulators which will be referred to as pristine insulators. Fig. 7 shows the setup for conducting electrical withstand testing on the insulator. The testing transformer can produce up to 250 kV of power frequency voltages. The transformer is connected with a voltage

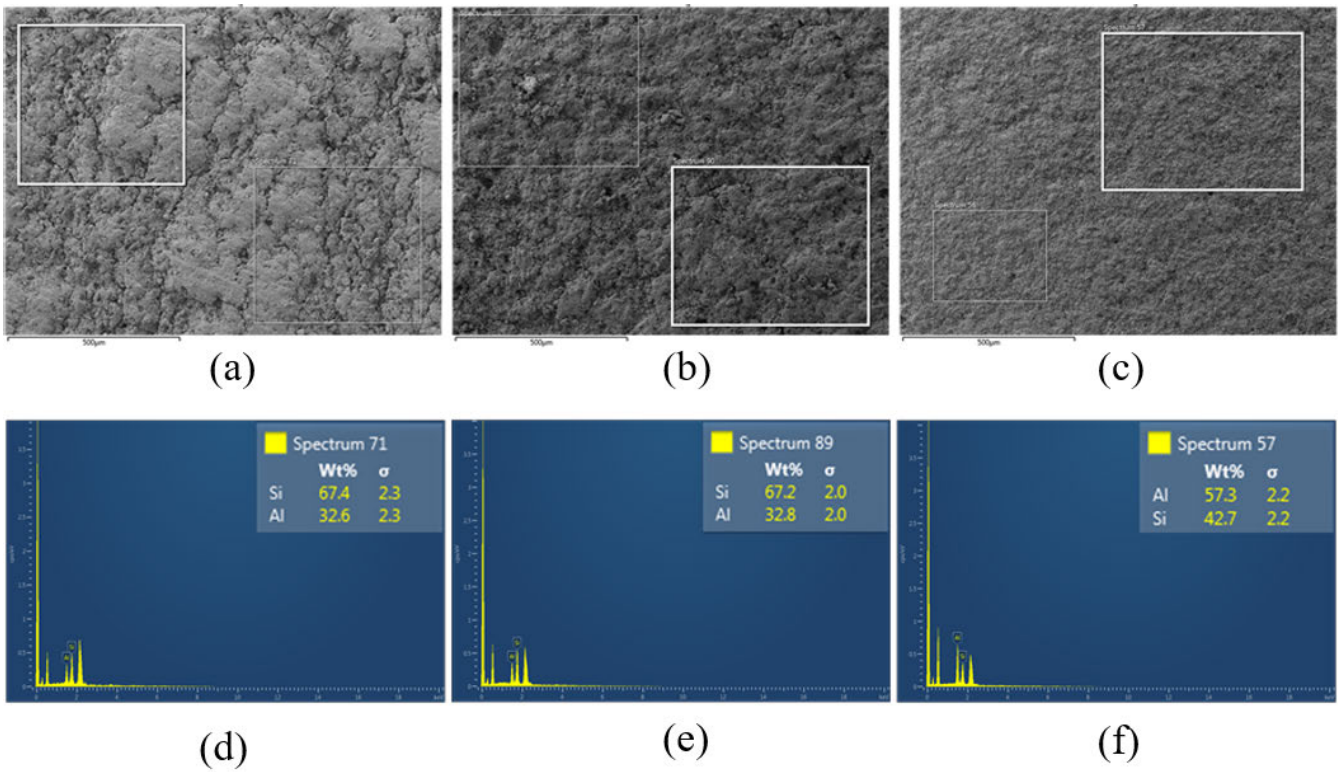

FIGURE 6. SEM and EDX anlysis results analyzing the material degradation of composite HVI after the service life of ten years. (a), (b), (c), SEM results from the samples obtained from field aged composite HVIs. All the samples exhibit a coarse and rough surface morphology, indicating widespread surface damage. (d), (e), (f) EDX analysis results at accelerating voltage of 9 kV showing a marked drop in Si/Al ratio compared to pristine sample for all the field aged insulators.

regulator to produce the variable output voltage. The fog chamber is design as per IEC 60507.

Due to limitation of our test source, the withstand test was performed on an equivalent arc length of one meter from the high voltage end. A phase to ground voltage of 60 kV was initially applied to prevent any overvoltage resulting from switching transients. Steam generator producing steam fog with a rate of 0.05 kg/h/m3 of test chamber was turned on after the applicaiton of test voltage. After a delay of twenty minutes, during which the fog chamber was also filled with steam, the voltage was increased in step size of ten percent with an interval of five minutes until flashover was observed. Just before flashover severe dryband arcing and leakage current was observed with a peak-peak magnitude of up to 52 mA. Some of the contaminants were washed away due to condensation. The voltage step below the flashover voltage was considered to be the withstand level for the field insulators. Fig. 8 illustrates the progressive stress testing procedure conducted to assess the dielectric strength of the insulator [57].

It is pertinent to note that repetitive test procedures are not suitable for field insulators due to risk of losing natural pollution in presence of steam fog. Table 4 summarizes the electrical withstand performance of the field insulators. It can be seen that the performance of the field insulators has decreased due to the ageing phenomena. The insulators were rated to withstand 1228 kV under wet conditions, but after field service of 10 years, their withstand voltage has shown a reduction of up to 30 % which is expected after the drop in hydrophobicity class [58].

TABLE 4. Comparison between Rated Withstand Voltage and Observed Withstand Voltage of Field Aged Insulators.

Sample	Rated Withstand Voltage (kV)	Withstand Voltage for 1 m section (kV)	Extrapolated Withstand Voltage (kV)
FS001	1228	188	856
FS002	1228	207	943
FS003	1228	188	856

F. HYDROPHOBICITY INVESTIGATIONS

The primary strength of composite HVI lies in its inherent capacity to prevent the formation of continuous moisture films on its surface. This surface quality resists the creation of conductive pathways, resulting in low leakage current, reduced flashover risks, and minimized deterioration from tracking when compared to ceramic insulators. This characteristic, known as hydrophobicity, significantly contributes to the superior performance of composite HVIs in highly contaminated environments, including coastal and industrial areas [59]. However, as the composite material undergoes

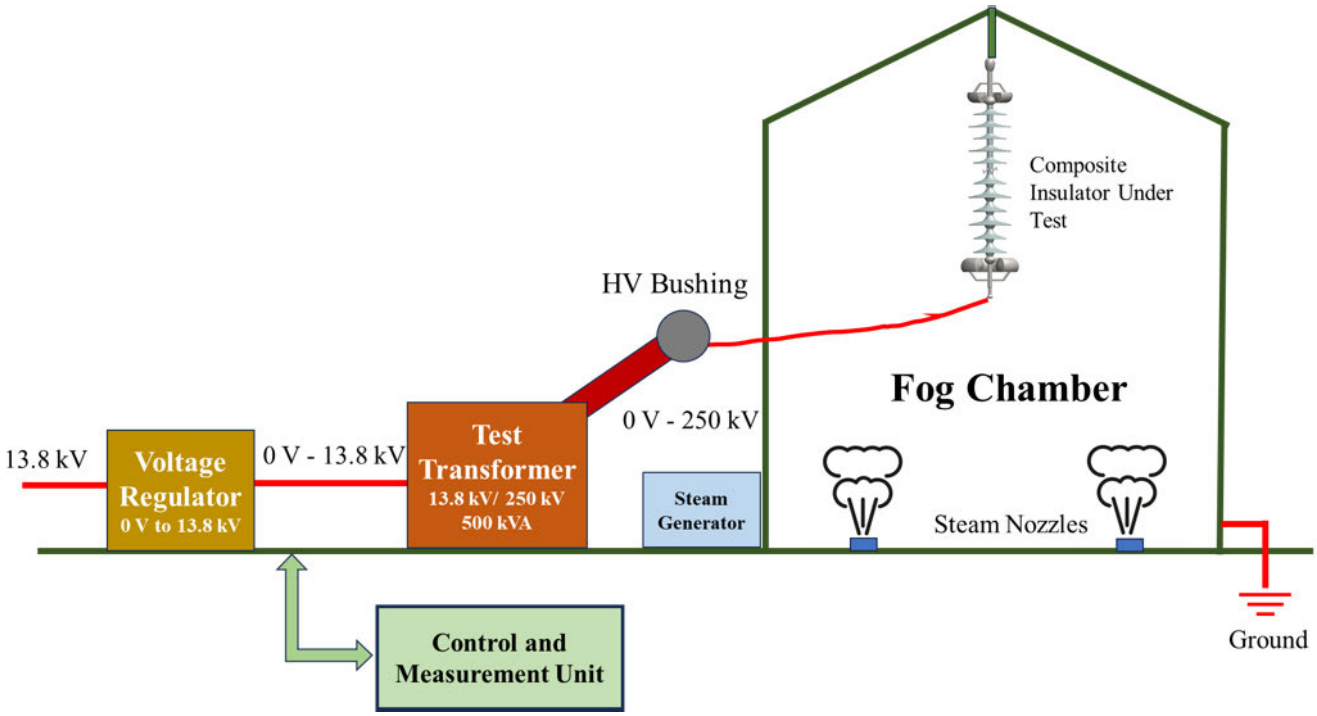

FIGURE 7. Electrical test setup with fog chamber and steam generator to perform clean fog test as per IEC 60507.

aging in the field, coupled with the surface deterioration discussed in Section II-C, it is highly likely that the hydrophobic properties of the composite insulator will diminish [60], [61].

According to IEC 62073, the hydrophobicity of composite insulators can be measured using one of the following methods [49]. These methods include: (a) Spray Method, (b) Contact Angle Method, and (c) Surface Tension Method. Spray method is widely used for hydrophobicity measurement in HV labs throughout the world because it is simpler to perform and require basic equipment. This method includes spraying distilled water on the insulator surface. The surface is carefully photographed and photos are compared to standard photos included in IEC 62073 to determine the hydrophobicity class. Hydrophobicity class of the surface is determined by the operator based on this comparison. The hydrophobicity classes of the insulators are divided from HC1 to HC7 with HC1 associated with pristine insulators which are new and not exposed to environmental effects and UVR. Table 5 summarizes the different hydrophobicity class levels and what each class level means and tells about the insulating surface.

To investigate the loss in hydrophobicity in field insulators, we performed surface hydrophobicity tests for both the pristine insulators and field aged insulators made by same manufacturer. Fig. 9 shows the comparison of hydrophobicity levels for pristine and field insulators. Fig. 9 (a) shows the hydrophobicity performance of pristine insulator with hydrophobicity class of HC1. It can be seen in Fig. 9 (a) that the discrete water droplets are formed, with most having a perfectly circular shape. However, a few droplets with

TABLE 5. Hydrophobicity Classes and their Interpretations.

Hydrophobicity Class	Meaning
HC1	Discrete Drops of circular shape
HC2	Discrete Drops with regular shape deviating from circular
HC3	Discrete Drops with irregular shape
HC4	Both Discrete Drops and wetted traces or films (less than 10%)
HC5	Both Discrete Drops and water films (more than 10% but under 90%)
HC6	Water films (more than 90% but under 100%)
HC7	Continuous water film

irregular shape can also be noticed in Fig. 9. Fig. 9 (b) shows the hydrophobicity levels of field aged composite insulators with the hydrophobicity class of HC5. The shape of water droplets are no longer round and spherical. They are flat with very deformed shapes. Also, the surface area they acquire is larger. Moreover, the bottom of sheds did not show wetting in both cases unless the spray nozzle was intentionally pointed towards them. This deterioration of HC levels of field insulators will increase the leakage current across the insulator surface.

The effect of these deformed water droplets due to loss in hydrophobicity will increase the leakage current which increases the dry band arcing across the insulator. However, will this phenomena also effect the electric field distribution and intensity across the insulator? Can this phenomena also result in increase in corona formation across the insulator.

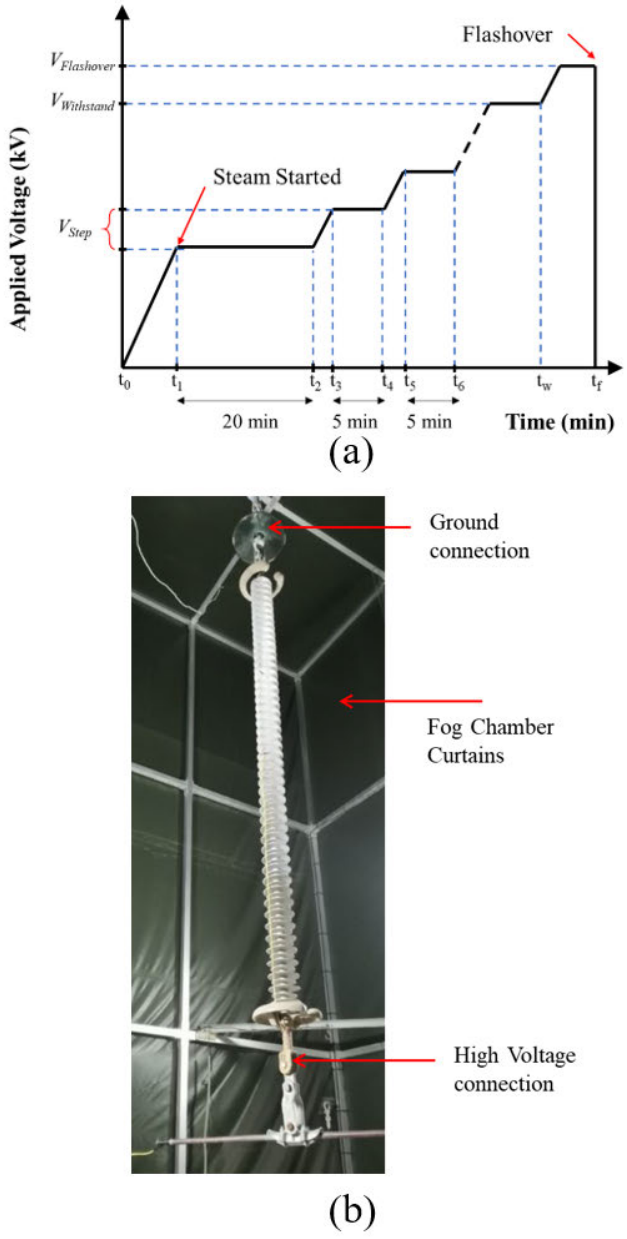

FIGURE 8. (a) Progressive Stress Method for electrical testing. Voltage is increased in steps of ten percent,(b) A field aged insulator being tested in the fog chamber.

These questions need to be investigated thoroughly and are the primary research objective of the proposed research work.

One of the focus areas of this research work includes the investigation of effect of poor hydrophobicity class on the electric field intensity and dielectric stress across the composite insulators. It is the electric field distribution which eventually ionizes the air around the insulator and results in flashover and compete loss of insulation. Therefore, the second half of this paper deals with investigating the effects of hydrophobicity on electric field distribution.

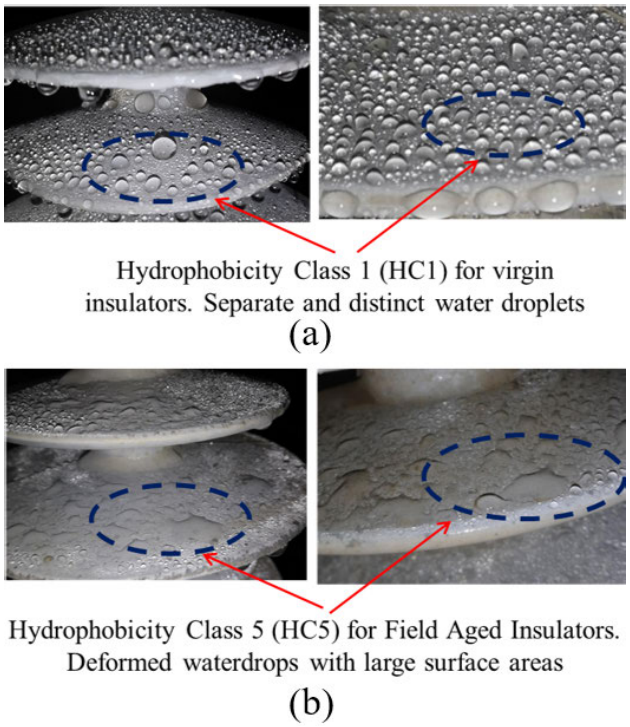

FIGURE 9. Hydrophobicity Analysis for (a) Pristine Insulator with Hydrophobicity Class 1 (HC1), and (b) Field Aged Insulator with Hydrophobicity Class 5 (HC5).

III. HYDROPHOBICITY AND DIELECTRIC STRESS

This section discusses the theoretical background of hydrophobicity phenomena and how it can contribute in increase in the electric field intensity across the insulator and intensify dielectric stress.

A. BACKGROUND

It has been observed that water droplets accumulate on the surface of composite insulator due to rain and humidity. These water droplets tend to distort the electric field distribution around the composite insulator [62]. To develop an analytical understanding of this effect, consider a single droplet of water lying on a composite surface between HV and ground electrodes as shown in Fig. 10. Without the presence of water droplet, electric field lines between these electrodes are weakly uniform. Since, the relative permittivity of water is much higher than SiR and air, the electric field travelling through the air and SiR tends to enter the water droplet resulting in concentration of electric field around the droplet. This phenomenon has been explained in literature as the presence of triple junction i.e., air, water, and SiR [63], [64], [65], [66].

However, it is important to understand, what happens to the electric field as it enters the water droplet. As shown in Fig. 11 (a), as the electric field vector E_2 enters the water droplet, it deviates from its original path and transforms into a field vector E_1 with a different magnitude. The following mathematical analysis help to understand the reason for this

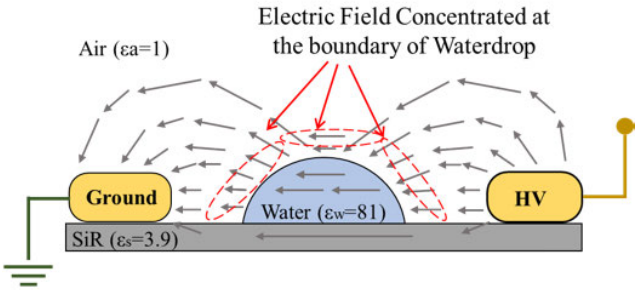

FIGURE 10. Analysis of field intensification using single droplet on surface of SiR, lying between HV and Ground electrodes. The Electric Field concentrates close to the single droplet resulting in electric field intensity in those regions.

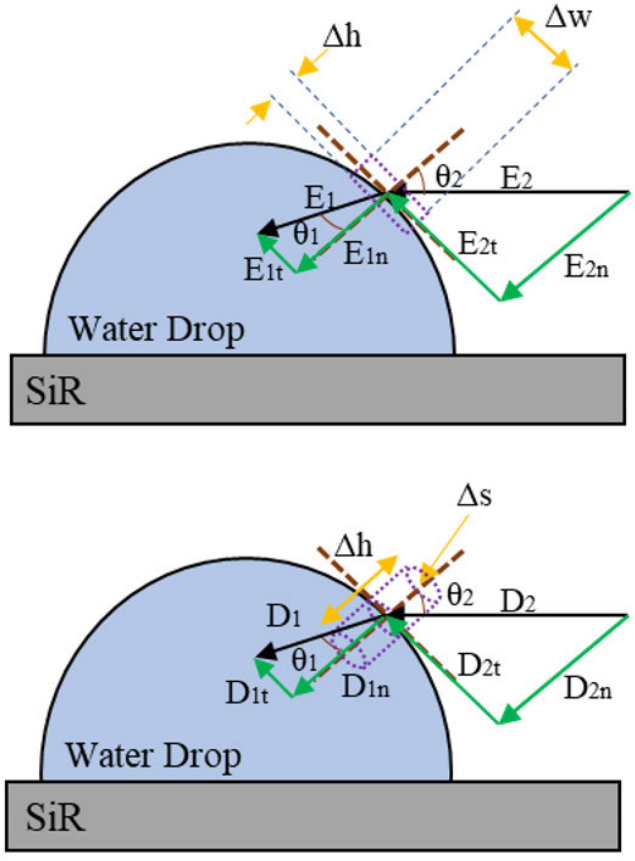

FIGURE 11. Analysis of field intensification using single droplet on surface of SiR, lying between HV and Ground electrodes (a) Electric field across the boundary of air and water droplet (b) Electric flux density across the boundary of air and water droplet.

change in magnitude and develop an intuitive understanding regarding the magnitude of change. Considering, faradays law of electromagnetic induction (1) and applying it to rectangular boundary defined in Fig. 11 (a) yields (2).

$$\oint E.dl = 0 \tag{1}$$

$$E_{1t}\Delta w - \frac{E_{1n}\Delta h}{2} - \frac{E_{2n}\Delta h}{2} - E_{2t}\Delta w + \frac{E_{2n}\Delta h}{2} + \frac{E_{1n}\Delta h}{2} = 0 \tag{2}$$

where E_t is the tangential component of the electric field, and E_n is the normal component of the electric field, Δw and Δh are the width and height of the closed boundary respectively. As $\Delta h \to 0$,

$$E_{1t} = E_{2t} \tag{3}$$

Equation (3) indicates that tangential component of electric field is not impacted when field lines enter the water droplet. Conversely, normal component of electric field undergoes a change. We can rewrite (3) in terms of electric flux density D as shown in (4).

$$\frac{D_{1t}}{\epsilon_0\epsilon_w} = \frac{D_{2t}}{\epsilon_0\epsilon_a} \tag{4}$$

where D_t is the tangential component of electric flux density, and ϵ_a and ϵ_w are the permittivity of air and water, respectively. It can be clearly noticed that the tangential component of electric flux density does not remain the same when entering the water droplet.

Applying gauss's law (5) to a cylindrical boundary drawn in Fig. 11 (b), results in equation (6).

$$\oint D.ds = Q_{enc} \tag{5}$$

$$Q = \rho_s\Delta s = D_{1n}\Delta s - D_{2n}\Delta s \tag{6}$$

where Δ_s is the cross-sectional areas of the cylinder, D_n is the normal component of flux density and ρ_s is the charge density at the boundary. Assuming, there are no free charges in the water droplet and the surface charge density at the boundary i.e., ρ_s is zero. This implies that the normal component of electric flux density remains unchanged across the boundary of water as shown in (7).

$$D_{1n} = D_{2n} \tag{7}$$

Equation (7) can be rewritten in terms of electric field intensity (8) and rearranging it we can obtain (9) which indicate the relative strength of E_2 and E_1.

$$\epsilon_0\epsilon_w E_{1n} = \epsilon_0\epsilon_a E_{2n} \tag{8}$$

$$E_{1n} = \frac{\epsilon_a}{\epsilon_w}E_{2n} \tag{9}$$

Considering significantly high relative permittivity of water, the electric field E_{1n} inside the water droplet is significantly weaker than the field outside it. However, to develop a better understanding of the physical phenomenon taking place and to obtain exact numerical results, the analytical approach described here is insufficient and numerical simulations have for calculation of electric field have been carried out in COMSOL Multiphysics as shown in the following sections [67], [68].

B. SINGLE DROPLET CONTRIBUTION IN DIELECTRIC STRESS

To develop a better understanding of the impact of water droplet on electric field distribution, we have carried out

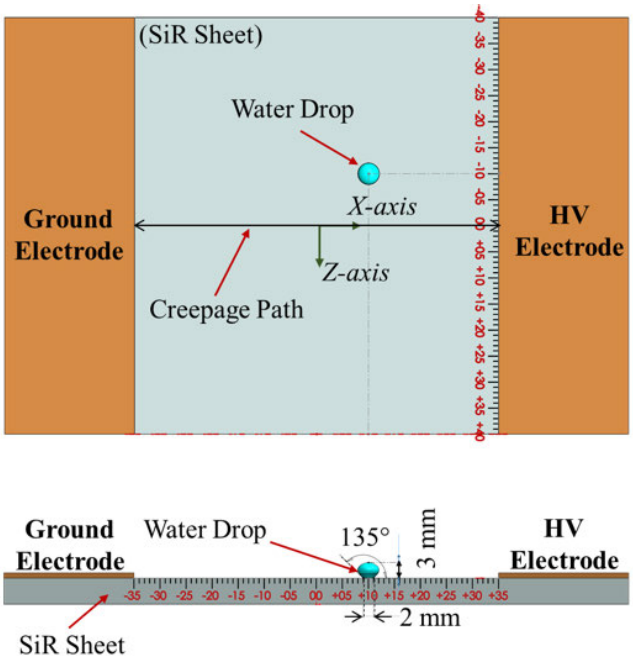

FIGURE 12. A 5 mm thick SIR sheet 120 mm* 80 mm. 1mm thick copper electrode 25 mm*80 mm (in brown) is used as HV and ground electrode.

simulation analysis in COMSOL multiphysics using a simplified single drop model as shown in Fig. 12. A 5 mm thick SiR sheet with dimensions 120 mm* 80 mm is used as the insulator. 1mm thick copper electrode with dimensions of 25 mm*80 mm (in brown) are used as High Voltage (HV) and ground electrode. 1700 V is applied to HV electrode to achieve a specific creepage distance (SCD) of approximately 41 mm/ kV, i.e., equal to our field aged insulator.

The electric field distribution between two parallel plates is expected to be weakly uniform in the absence of a water droplet. However, when a water droplet is placed at the center of the sheet, the electric field becomes concentrated and intensified around the droplet, as illustrated in Fig. 13 using an arrow volume plot. The field lines concentrate around the droplet due to its significantly high relative permittivity. However, a closer look in Fig. 13(c) reveals that the field strength inside the droplet is rather low, which aligns with the mathematical understanding in equation (9). The intensification of the electric field at the boundary of the water droplet consequently contributes to the ionization of the air surrounding the droplet, potentially leading to a flashover if this intensification spreads widely and becomes substantial.

To further investigate and quantify the effect of size and location of the droplet on electric field intensification a series of simulations have been carried out with a single droplet model. As shown in Fig. 12, the water droplet has a height of 3 mm, waterdrop surface contact diameter is 2 mm, and it has a contact angle of 135 degrees indicating a highly hydrophobic SiR surface.

Firstly, the water droplet is moved along the z-axis while maintaining its x-axis position at zero. The results are

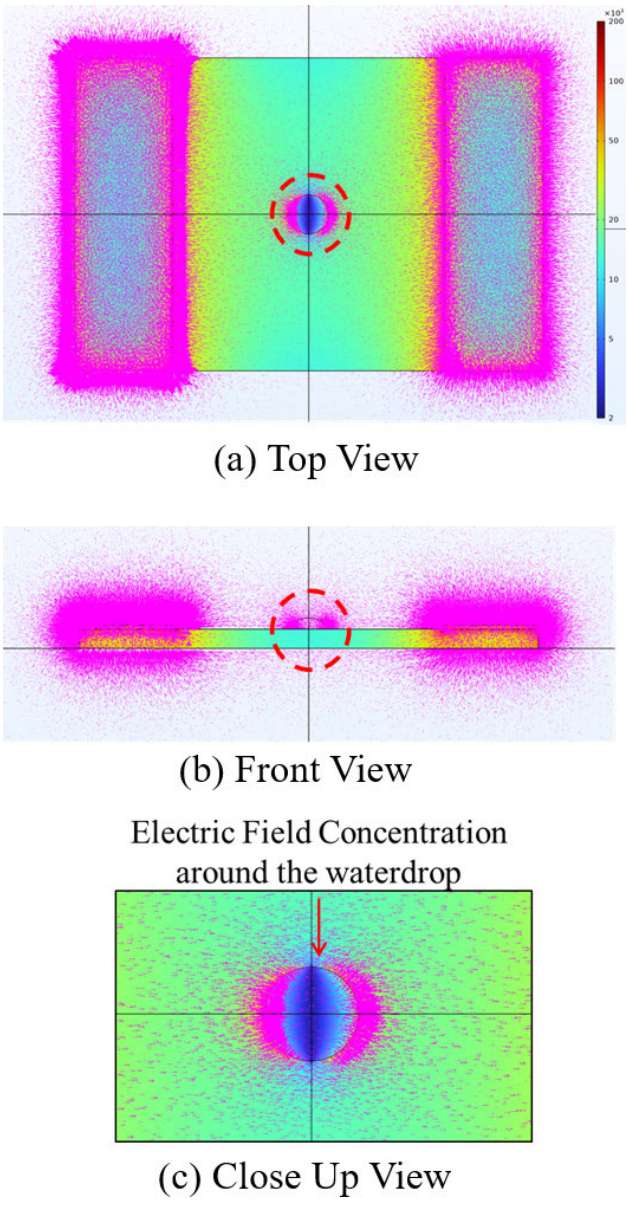

FIGURE 13. A single water droplet is centered on the SiR surface between a HV and Ground Electrode. Pink arrows represent Electric Field.

depicted in Fig. 14. The electric field is measured along the creepage path indicated in Fig. 12, which extends from the HV electrode to the ground electrode, running along the center of the SiR surface. When the water droplet is positioned directly along the creepage path (0 mm), the field intensification is at its highest, as expected. However, as the droplet is shifted away from the creepage path, the degree of field intensification gradually diminishes. At 7 mm, there is virtually no discernible effect of the water droplet on the electric field distribution. Placing the droplet along the creepage path results in significantly lower field intensity underneath it. This observation aligns with previous findings, indicating that the electric field intensity beneath the water

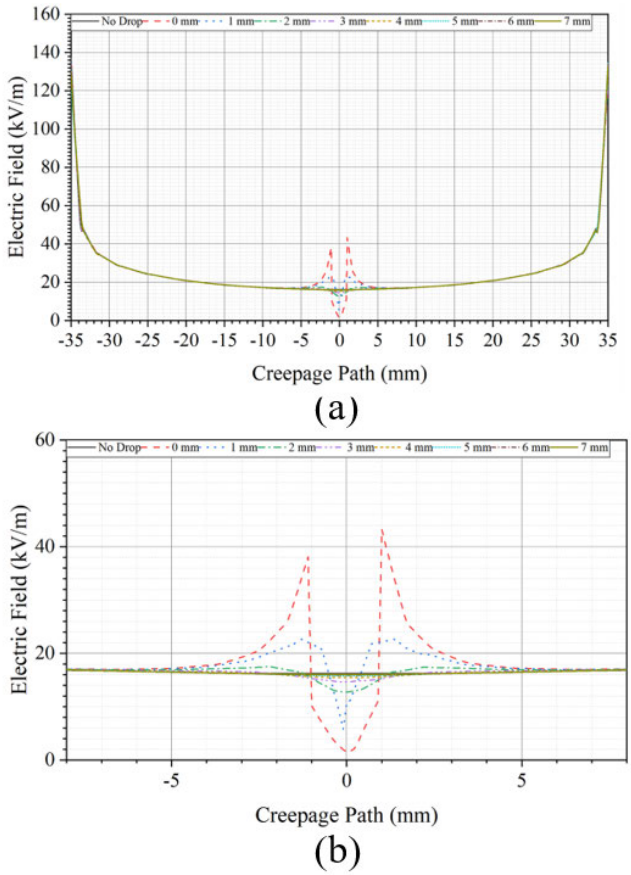

FIGURE 14. (a) Electric Field is measured along creepage path. The drop is displaced in z axis (x=0), (b) The closeup view depicting intensification of electric field when water droplet is close to the creepage path.

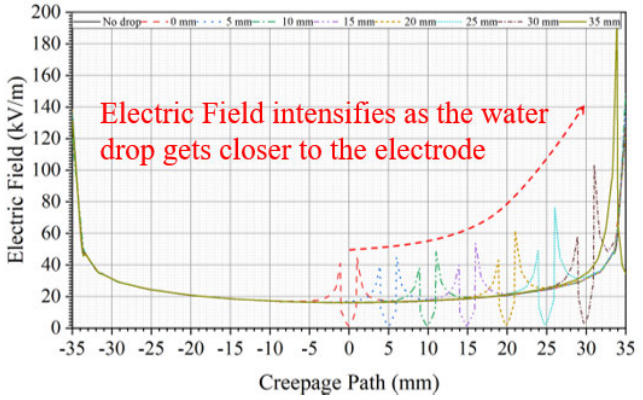

FIGURE 15. Electric Field is measured along creepage path. The drop is displaced in x axis (z=0).

droplet tends to be lower than in cases where no droplet is present.

Secondly, the water droplet is moved along the x-axis while maintaining its z-axis position at zero. The results are illustrated in Fig. 15. The electric field is measured along the creepage path. Initially, the water droplet is centered, and then it is gradually shifted toward the HV electrode. In each case, the most significant field intensification is observed at the boundary of the water droplet. Furthermore, the field intensification at the boundary closer to the electrode is relatively higher than at the other boundary. Notably, field intensification becomes more pronounced as the droplet moves nearer to the electrode. Throughout these variations, the electric field intensity beneath the water droplet remains significantly lower. This observation aligns with our previous findings and theoretical understanding.

Furthermore, practical observations in Fig. 9 reveal that the size of water droplets on highly hydrophobic SiR is not constant. As the volume of spray increases, smaller water droplets close to each other tend to combine and form larger droplets. Hence, it's crucial to understand the impact of droplet size on field intensification. We placed the water droplet at the origin and varied its diameter from 2 mm to 16 mm. Field intensification becomes more significant as the droplet size increases, as depicted in Fig. 16 (a) and (b). Once again, it's clear that the field intensity beneath the droplet is much lower, in line with previous observations. Additionally, we made an observation regarding the potential distribution, as shown in Fig. 16 (c) add (d). It reveals that the potential gradient beneath the droplet becomes relatively low, which aligns with the reduction in electric field under the droplet.

C. MULTIPLE DROPLETS CONTRIBUTION IN DIELECTRIC STRESS

In Section III. b we have investigated the distortion of electric field distribution across an insulator due to a single waterdrop on the surface of that insulator. We carried out further investigations to understand the effect of multiple waterdrops on electric field distribution between electrodes. As we have seen in Section II-F and in Fig. 9, the multiple water droplets that are formed on composite insulators vary in shape and size according to the hydrophobicity class of the insulator surface. This effect is shown in Fig. 17 where two multiple water droplet scenarios on SiR sheet are simulated between parallel electrodes having uniform field distribution between them.

Fig. 17 (a) shows multiple waterdrops with spherical shape as expected to be found on pristine insulator surface with hydrophobicity class HC1 and shown in Fig. 9. It can be seen that due to the spherical shape and small size of waterdrops, the concentration of field is not significant. However, in the case of large waterdrops as shown in Fig. 17 (b), the electric field concentration across the deformed waterdrops is high. This scenario is also depicted in Fig. 18 which shows the electric field intensity across the creepage length of the insulator. Fig. 18 clearly shows that due to presence of large deformed flat droplets across the insulator surface, the electric field distribution is no longer uniform and the electric field intensity has also intensified across the insulator in areas where deformed waterdrops exist.

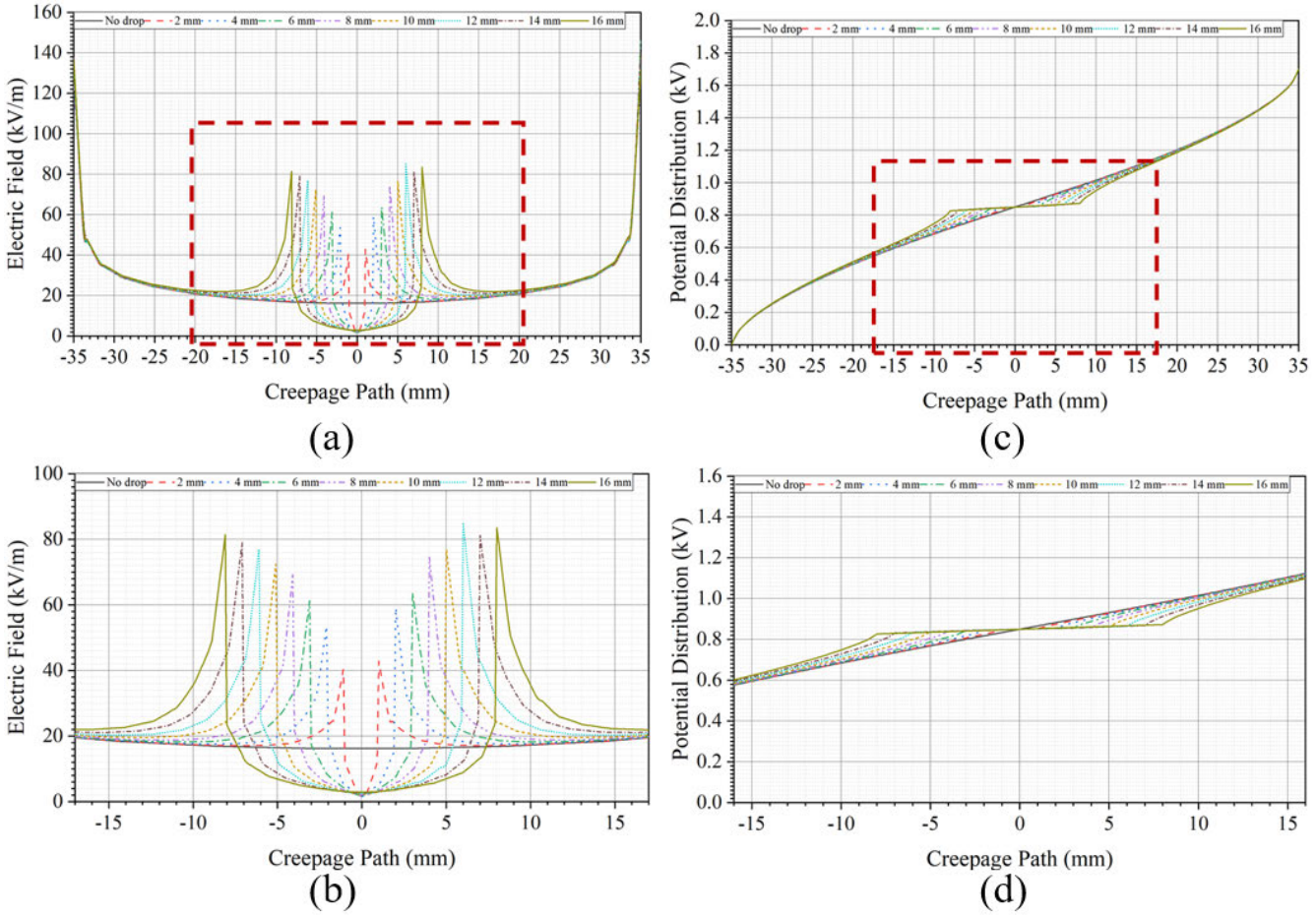

FIGURE 16. A single drop is placed at the origin and its diameter is varied (a) (b) Electric Field Measurement along creepage path which shows significant increase as the water diameter increases (b) Potential gradient beneath the water droplet remains low.

IV. DIELECTRIC STRESS ON FIELD AGED INSULATOR

To develop an understanding regarding the effect of hydrophobicity loss on an actual field aged insulator, we have designed its model in SOLIDWORKS and performed its electrostatic analysis in COMSOL Multiphysics. A pristine insulator model was designed as shown in Fig. 19 and then water droplets were added on it in different shapes, number and distribution as per the specification of HC1 and HC5 respectively.

A. MODELLING

The modelled insulator is shown in Fig. 4. The total length of the insulator is 4910.52 mm with an arc length of 4552 mm and creepage distance of 15458 mm. It is composed of total 92 sheds with 47 small and 45 large sheds. The material for the insulator is Silicone Rubber (SiR) with Fiber Glass rod. The insulator has forged steel corona rings at both ends and the electrodes are also made up of forged steel. Table 1 summarize all the physical properties of the modelled insulator. The materials selected for the insulator and their relative permittivity and conductivities are listed in Table 6.

TABLE 6. Materials and their Properties used for the Modeling of Composite Insulators [62].

Material	Relative Permittivity, ϵ_r	Conductivity, σ (S/m)
Silicone	3.9	1×10^{-12}
Glass Fibre	4.2	1×10^{-12}
Forged Steel	1	5.9×10^{7}
Water Droplets	81	180×10^{-6}

B. SIMULATION ANALYSIS FOR VARYING HYDROPHOBICITY

Numerical simulations were performed in COMSOL Multiphysics. Water droplets were created on the surface of insulator sheds to understand their effect on the potential distribution and electric field distribution around the HVI. This electric field establishes in the air around the energized insulator and is responsible for the ionization of air before the flashover across the insulator. The water droplet distribution was selected according to the standardized Hydrophobicity Classes (HC). Fig. 19 shows the water distribution across the field aged insulator with hydrophobicity class of HC5. These distributions were also inspired from the real water droplet distribution as shown in Fig. 9.

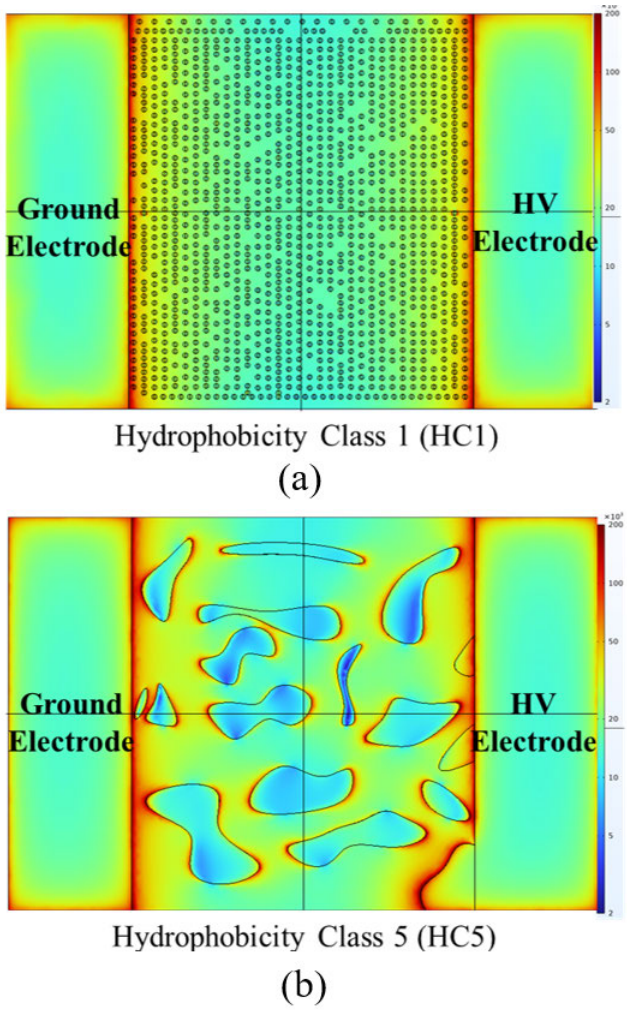

FIGURE 17. Surface plots for electric field comparison for different Hydrophobicity classes (a) Water distribution as found in HC1 (b) Water distribution as found in HC5.

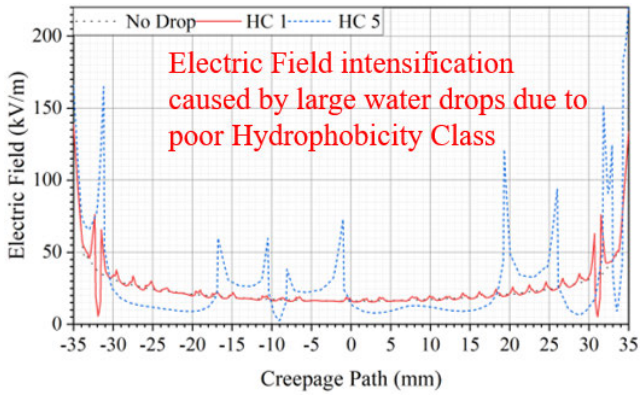

FIGURE 18. Electric field distibution along creepage length between the electrodes. Intensification of Electric Field can be observed due to poor hydrophobicity class HC5.

The insulator under research is composed of total 92 sheds with a length of almost 5 meters and it is almost impossible to show the complete insulator and present the results in

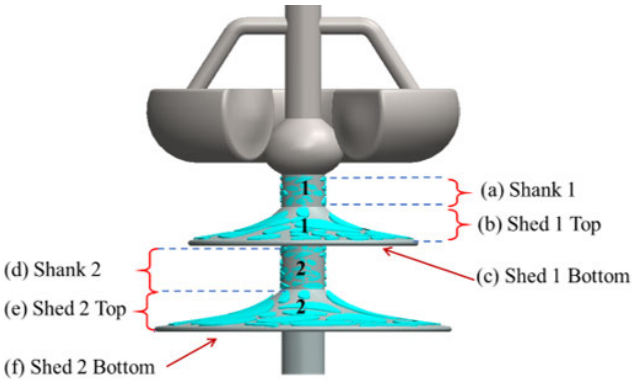

FIGURE 19. Modelled Insulator with HC5 level hydrophobicity.

pictorial form. Therefore, two sheds along with the ground electrode and corona ring were selected for detail analysis in the following sections. The choice of ground electrode was made since, the top surface of the sheds shows higher contamination levels and decreased hydrophobicity after ageing in field [69], [70]. The bottom surface of the sheds also show lower accumulation of water as discussed in 2.6. The field intensification phenomena across two sheds along with fundamental understanding developed in Section III-B, can be extrapolated for the whole insulator for further understanding.

Fig. 19 also shows different labelled regions which will be used to explain results in the corresponding section. The potential and electric field distribution is analyzed for the the two shank section marked as 1 and 2, and also for the top and bottom of two sheds marked as 1 and 2 as shown in Fig. 19.

The potential distribution across the insulators has been analyzed and is presented in Fig. 20. In Fig. 20 (a), the potential distribution across the pristine Insulator is shown, while Fig. 20 (b) displays the distribution across the Field Insulator. The linear distribution of voltage across the selected sheds is illustrated in Fig. 20 (c).

Fig. 19 highlights the marked regions on the insulator sheds, which are also visible on the linear graph in Fig. 20(c). These marked regions represent the shanks, the top of the sheds, and the bottom of the sheds.

In Fig. 20 (c), slight perturbations in the voltage distribution can be observed for HC1 and HC5 when compared to a dry insulator. The perturbations in the voltage distribution of HC5 are notably more pronounced and easily visible. Along the length of HC5, there are several places where the voltage gradient decreases, resulting in a relatively horizontal voltage curve. This observation aligns with the findings presented in Fig. 16, which demonstrates that the presence of a water droplet leads to a dip in the electric field and, consequently, a decrease in the potential gradient.

Fig. 21 shows electric field distribution across pristine and field insulators. It can be seen that for the field insulator with hydrophobicity levels of HC5, the electric field has intensified significantly across the insulator shed and shanks.

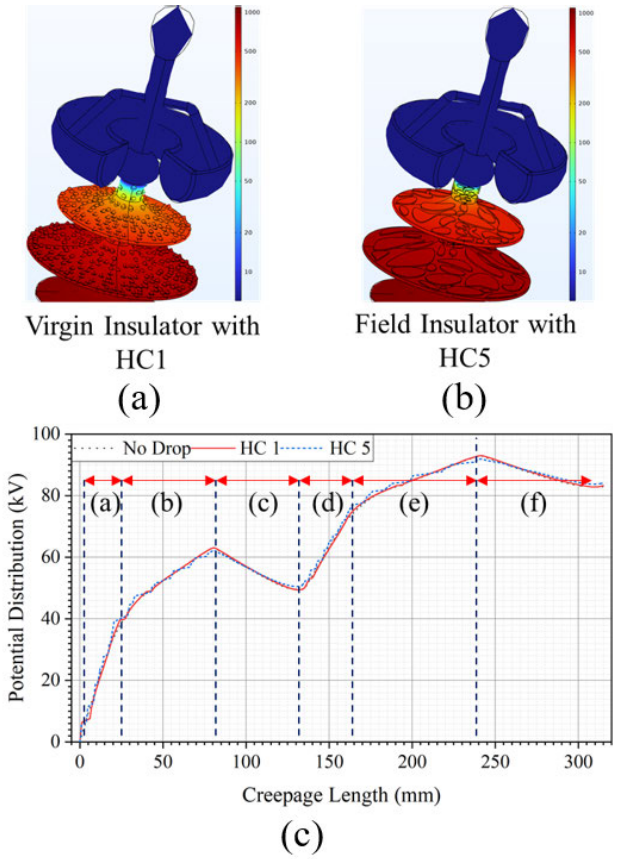

FIGURE 20. Potential distribution graphs (a) Surface plot for top two sheds with water distribution as per HC 1, (b) Surface plot for top two sheds with water distribution as per HC 5, (c) Comparison of HC 1, HC 5 and dry surface.

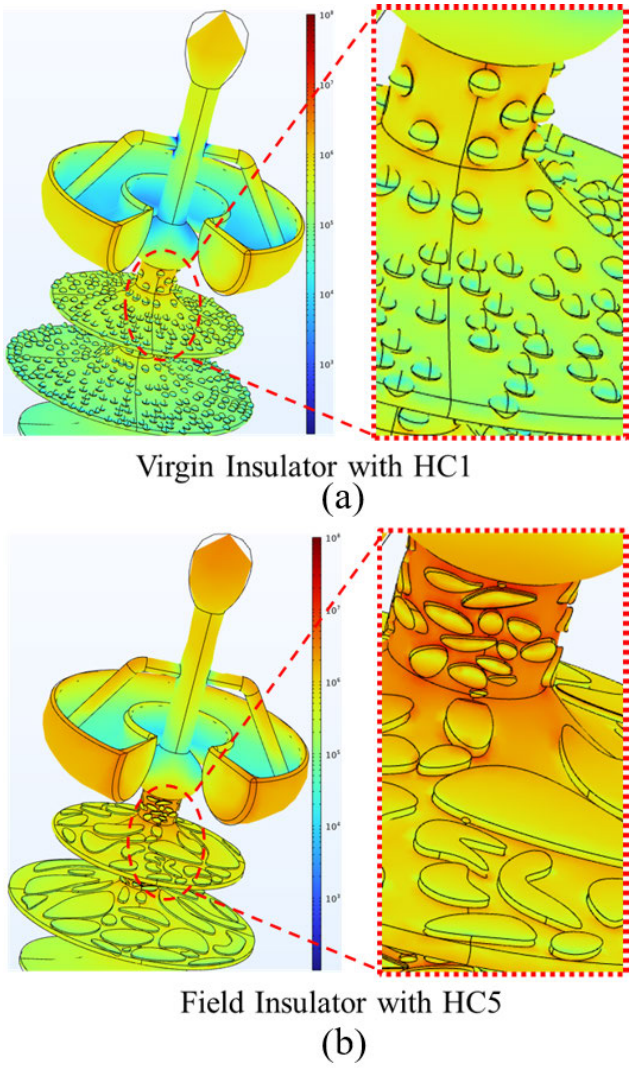

FIGURE 21. Electric field distribution across the wet pristine and wet field insulator (a) Water droplet distributions on sheds for HC1 level and electric field distribution across the waterdroplets(b) Water droplet distributions on sheds for HC5 level intensification of electric field across the water droplets.

This increase in electric field concentration is experienced across the insulator shank and also on sheds due to uneven water droplets. The intensification of electric field in these areas will result in ionization of the air in surrounding areas. This can lead to corona formation. It will also affect the insulation between the arc distance of the insulator and further increase the chances of flashover. The intensification of electric field due to poor levels of hydrophobicity is a very significant finding of our work as it also explains the field life of composite insulators. The poor hydrophobicity will lead to corona, which will consequently affect the composite surface and its hydrophobicity levels. It will result in cyclic chain reaction which will lead to quick deterioration of the insulator.

Another critical aspect which is identified in the findings is about the electric field intensification at the shank of the insulator as shown in Fig. 21 and and also in Fig. 22. The field intensification at the region a and d, shown in Fig. 22 which represent the shank region of insulators, will result in formation of corona at the shank of the insulator. This corona will further accelerate the deterioration of the composite material at the shanks and result in exposing the fiber glass rod. The fiber glass is not designed to withstand environmental stresses. The further deterioration of composite insulator shanks will seriously compromise its mechanical strength and it will result in hazardous situation by breaking up and consequently falling of HV conductor on the ground.

The intensification of the electric field intensity on field insulators due to poor hydrophobicity levels is clearly evident in Fig. 22. When HC5 hydrophobicity is compared with dry insulator and HC1, the field insulator is now subjected to higher electrical stresses. These stresses are due to deposition of uneven water droplets across the insulator surface which are causing intensification of electric field. The air surrounding these waterdrops are now subjected to higher stresses leading to corona formation and further deterioration of the SiR material. As previously discussed, the increase in corona will expose the fiber glass rod to UVR and it will seriously compromise the mechanical strength of the insulator.

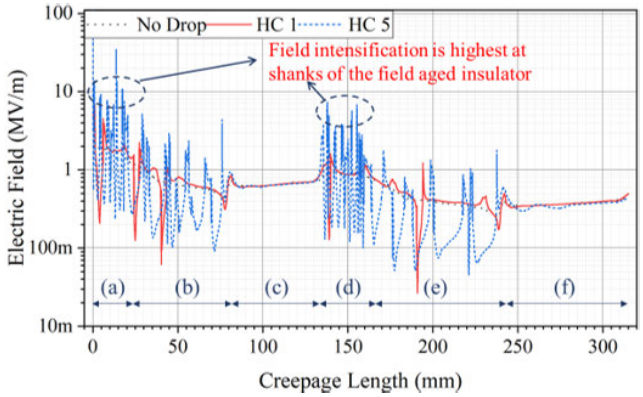

FIGURE 22. Line graph of electric field along creepage path. Comparison of HC 1, HC 5 and dry surface.

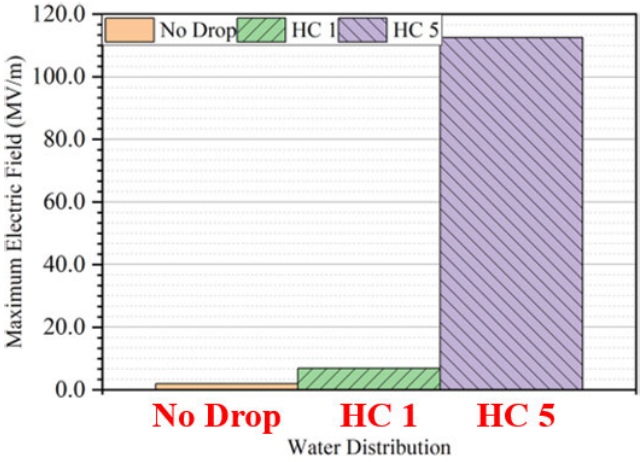

FIGURE 23. Bar graph showing the intensity levels of Electric Field Intensity on the pristine and field insulator.

Fig. 23 shows a bar graph comparing the maximum electric field intensity across the pristine and field insulator sheds when they are covered with water. It can be seen that accumulation of HC5 water droplets over the insulator has resulted in 1200 % or twelve times increase in electric field concentration in certain areas of the insulator. This enhanced electric field will lead to corona formation in these areas. The corona will eat up Silicone Rubber material of the composite insulator further deteriorating the hydrophobicity levels of the insulators. This explains one of the reasons why composite insulators have very short service life when compared to ceramic insulators as their deterioration rate keeps accelerating throughout the service life, and lost hydrophobicity, contributes significantly to this.

V. CONCLUSION

In this research paper, field aged insulators after serving ten years in the harsh environment of Saudi Arabian coastal regions are analyzed. The insulation material of field-aged insulator was investigated by SEM and EDX which indicated the deterioration of the insulator surface due to exposure to environmental conditions. As expected, this degradation of material also affected the hydrophobic properties of the composite HVI which were investigated through hydrophobicity tests and comparison with new insulators of the same material. The field insulators have shown hydrophobicity class of HC5 which results in intense leakage current when covered with contaminants and water. Moreover, the effects of water accumulated on surface of insulators on the electric field distribution across the insulator is analyzed through simulations in COMSOL. It was observed that the poor hydrophobicity of insulators also resulted in electric field intensification on the surface of insulators. Finally, the composite insulators having hydrophobic properties of pristine insulators and field aged insulators are modelled and simulated to study the potential distribution and electric field distribution across the insulator. It was observed that the electrical field distribution across the insulators becomes more non-uniform and is enhanced at particular areas around the contaminated insulator with poor hydrophobicity. This enhancement in electrical field intensity results in Corona inception across the insulators causing accelerated degradation of the composite material. This can lead to physical breakdown and flashover of the insulators. The presented work will act as resource for both the academic researchers and manufacturers about the performance of composite HVI in the field. It will also act as guide to understand the effects of changing hydrophobicity on the electric field distribution which can cause further ageing, can result in flashovers at operational voltages, and can also result in physically breaking of the HVIs.

REFERENCES

[1] Q. Zhao, X. Qi, M. Hua, J. Liu, and H. Tian, "Review of the recent blackouts and the enlightenment," in *Proc. CIRED Berlin Workshop (CIRED)*, vol. 2020, Sep. 2020, pp. 312–314.
[2] *Selection and Dimensioning of High-Voltage Insulators Intended for Use in Polluted Conditions—Part 1: Definitions, Information and General Principles*, IEC Standard 60815-1, Int. Electrotech. Commission, Worcester, MA, USA, 2008.
[3] N. Sharma, A. Acharya, I. Jacob, S. Yamujala, V. Gupta, and R. Bhakar, "Major blackouts of the decade: Underlying causes, recommendations and arising challenges," in *Proc. 9th IEEE Int. Conf. Power Syst. (ICPS)*, Dec. 2021, pp. 1–6.
[4] E. Bompard, T. Huang, Y. Wu, and M. Cremenescu, "Classification and trend analysis of threats origins to the security of power systems," *Int. J. Electr. Power Energy Syst.*, vol. 50, pp. 50–64, Sep. 2013.
[5] M. Rosas-Casals and R. Solé, "Analysis of major failures in Europe's power grid," *Int. J. Electr. Power Energy Syst.*, vol. 33, no. 3, pp. 805–808, Mar. 2011.
[6] R. J. Lings, "EPRI AC transmission line reference book-200 kV and above," Electr. Power Res. Inst., Palo Alto, CA, USA, Tech. Rep. 000000003002012636, 2005.
[7] E. A. Cherney, A. C. Baker, J. Kuffel, Z. Lodi, A. Phillips, D. G. Powell, and G. A. Stewart, "Evaluation of and replacement strategies for aged high voltage porcelain suspension-type insulators," *IEEE Trans. Power Del.*, vol. 29, no. 1, pp. 275–282, Feb. 2014.
[8] H.-P. Chao and R. Wilson, "Coordination of electricity transmission and generation investments," *Energy Econ.*, vol. 86, Feb. 2020, Art. no. 104623.
[9] R. S. Gorur, D. Shaffner, W. Clark, and R. Vinson, "Utilities share their insulator field experience," *Transmiss. Distrib. World*, vol. 57, no. 4, pp. 17–27, 2005.
[10] M. Plieva, E. Gurieva, and E. Lysokon, "Analysis of different modes of cleaning insulators of air transmission lines in mountain conditions," in *Proc. Int. Ural Conf. Electr. Power Eng.*, Sep. 2020, pp. 318–323.

[11] A. El-Hag, "Application of machine learning in outdoor insulators condition monitoring and diagnostics," *IEEE Instrum. Meas. Mag.*, vol. 24, no. 2, pp. 101–108, Apr. 2021.

[12] S. Anjum, S. Jayaram, A. El-Hag, and A. N. Jahromi, "Detection and classification of defects in ceramic insulators using RF antenna," *IEEE Trans. Dielectr. Electr. Insul.*, vol. 24, no. 1, pp. 183–190, Feb. 2017.

[13] M. F. Palangar, S. Mohseni, A. Abu-Siada, and M. Mirzaie, "Online condition monitoring of overhead insulators using pattern recognition algorithm," *IEEE Trans. Instrum. Meas.*, vol. 71, pp. 1–11, 2022.

[14] A. Ibrahim, A. Dalbah, A. Abualsaud, U. Tariq, and A. El-Hag, "Application of machine learning to evaluate insulator surface erosion," *IEEE Trans. Instrum. Meas.*, vol. 69, no. 2, pp. 314–316, Feb. 2020.

[15] L. Maraaba, Z. Alhamouz, and H. Alduwaish, "A neural network-based estimation of the level of contamination on high-voltage porcelain and glass insulators," *Electr. Eng.*, vol. 100, no. 3, pp. 1545–1554, Aug. 2017.

[16] L. Maraaba, K. Al-Soufi, T. Ssennoga, A. Memon, M. Worku, and L. Alhems, "Contamination level monitoring techniques for high-voltage insulators: A review," *Energies*, vol. 15, no. 20, p. 7656, Oct. 2022.

[17] L. Cui and M. Ramesh, "Prediction of flashover voltage using electric field measurement on clean and polluted insulators," *Int. J. Electr. Power Energy Syst.*, vol. 116, Mar. 2020, Art. no. 105574.

[18] J. S. Forrest, "The characteristics and performance in service of high-voltage porcelain insulators," *J. Inst. Electr. Eng. I, Gen.*, vol. 88, no. 11, pp. 414–418, Nov. 1941.

[19] S. Kumara and M. Fernando, "Performance of outdoor insulators in tropical conditions of Sri Lanka," *IEEE Elect. Insul. Mag.*, vol. 36, no. 4, pp. 26–35, Jul. 2020.

[20] J. Johnson, R. T. Henderson, W. S. Price, D. E. Hedman, and F. J. Turner, "Field and laboratory tests of contaminated insulators for the design of the state electricity commission of Victoria's 500-kY system," *IEEE Trans. Power App. Syst.*, vol. PAS-87, no. 5, pp. 1216–1239, May 1968.

[21] Z. Jiang, X. Jiang, Y. Guo, Y. Hu, and Z. Meng, "Pollution accumulation characteristics of insulators under natural rainfall," *IET Gener., Transmiss. Distrib.*, vol. 11, no. 6, pp. 1479–1485, Mar. 2017.

[22] Z. Zhang, X. Liu, X. Jiang, J. Hu, and D. W. Gao, "Study on AC flashover performance for different types of porcelain and glass insulators with non-uniform pollution," *IEEE Trans. Power Del.*, vol. 28, no. 3, pp. 1691–1698, Jul. 2013.

[23] X. Jiang, J. Yuan, L. Shu, Z. Zhang, J. Hu, and F. Mao, "Comparison of DC pollution flashover performances of various types of porcelain, glass, and composite insulators," *IEEE Trans. Power Del.*, vol. 23, no. 2, pp. 1183–1190, Apr. 2008.

[24] L. Yang, Y. Hao, L. Li, and Y. Zhao, "Comparison of pollution flashover performance of porcelain long rod, disc type, and composite UHVDC insulators at high altitudes," *IEEE Trans. Dielectr. Electr. Insul.*, vol. 19, no. 3, pp. 1053–1059, Jun. 2012.

[25] A. Allahdini, G. Momen, F. Munger, S. Brettschneider, I. Fofana, and R. Jafari, "Performance of a nanotextured superhydrophobic coating developed for high-voltage outdoor porcelain insulators," *Colloids Surf. A, Physicochem. Eng. Aspects*, vol. 649, Sep. 2022, Art. no. 129461.

[26] J. M. Seifert, W. Petrusch, and H. Janssen, "A comparison of the pollution performance of long rod and disc type HVDC insulators," *IEEE Trans. Dielectr. Electr. Insul.*, vol. 14, no. 1, pp. 125–129, Feb. 2007.

[27] F. M. Zedan, M. Akbar, A. S. Farag, T. C. Cheng, and C. Y. Wu, "Review performance of HV transmission line insulators in desert conditions Part I: Review of research and methods adopted internationally," *IEEE Trans. Electr. Insul.*, vol. EI-18, no. 2, pp. 97–109, Apr. 1983.

[28] M. Akbar, F. M. Zedan, M. A. Abdul-Majeed, and K. Y. Al-Soufi, "Design of HV transmission lines to combat insulator pollution problems in the eastern region of Saudi Arabia," *IEEE Trans. Power Del.*, vol. 6, no. 4, pp. 1912–1921, Oct. 1991.

[29] M. Akbar and F. M. Zedan, "Performance of HV transmission line insulators in desert conditions. III. Pollution measurements at a coastal site in the eastern region of Saudi Arabia," *IEEE Trans. Power Del.*, vol. 6, no. 1, pp. 429–438, Jan. 1991.

[30] F. M. Zedan and M. A. Akabar, "Performance of HV transmission line insulators in desert conditions. IV. Study of insulators at a semicoastal site in the eastern region of Saudi Arabia," *IEEE Trans. Power Del.*, vol. 6, no. 1, pp. 439–447, Jan. 1991.

[31] M. Z. Saleem and M. Akbar, "Review of the performance of high-voltage composite insulators," *Polymers*, vol. 14, no. 3, p. 431, Jan. 2022.

[32] A. Jermi, Y. He, and Q. U. Khan, "Performance of high-voltage polymeric insulators under simulated environmental conditions in desert areas of southern Libya," *Trans. Electr. Electron. Mater.*, vol. 19, no. 1, pp. 53–57, Jan. 2018.

[33] I. Y. Al-Hamoudi and Z. M. Al-Hamouz, "Reliability and cost effectiveness of silicone rubber insulators in the eastern coastal industrial area of Saudi Arabia," in *Proc. IEEE 10th Int. Conf. Transmiss. Distrib. Construct., Operation Live-Line Maintenance*, Apr. 2003, pp. 156–168.

[34] M. Amin, M. Akbar, and S. Amin, "Hydrophobicity of silicone rubber used for outdoor insulation (An overview)," *Rev. Adv. Mater. Sci.*, vol. 16, no. 1, pp. 10–26, 2007.

[35] J. Dadashizadeh Samakosh and M. Mirzaie, "Investigation and analysis of AC flashover voltage of SiR insulators under longitudinal and fan-shaped non-uniform pollutions," *Int. J. Electr. Power Energy Syst.*, vol. 108, pp. 382–391, Jun. 2019.

[36] L. S. Maraaba, K. Y. A. Soufi, L. M. Alhems, and M. A. Hassan, "Performance evaluation of 230 kV polymer insulators in the coastal area of Saudi Arabia," *IEEE Access*, vol. 8, pp. 164292–164303, 2020.

[37] M. R. Ahmadi-veshki, M. Mirzaie, and R. Sobhani, "Reliability assessment of aged SiR insulators under humidity and pollution conditions," *Int. J. Electr. Power Energy Syst.*, vol. 117, May 2020, Art. no. 105679.

[38] D. A. da Silva, E. C. M. da Costa, J. L. De Franco, M. Antonionni, R. C. de Jesus, S. R. Abreu, K. Lahti, L. H. I. Mei, and J. Pissolato, "Reliability of directly-molded polymer surge arresters: Degradation by immersion test versus electrical performance," *Int. J. Electr. Power Energy Syst.*, vol. 53, pp. 488–498, Dec. 2013.

[39] A. R. Verma and B. Subba Reddy, "Interpretation of surface degradation on polymeric insulators," *Eng. Failure Anal.*, vol. 95, pp. 214–225, Jan. 2019.

[40] H. Jiang, B. Li, B. Zhao, Q. Sun, C. Gao, and L. Chen, "Evaluation of aging process of silicone rubber composite insulators with photothermal radiometry," *J. Phys. D, Appl. Phys.*, vol. 51, no. 42, Sep. 2018, Art. no. 425304.

[41] S. M. Rowland, J. Robertson, Y. Xiong, and R. J. Day, "Electrical and material characterization of field-aged 400 kV silicone rubber composite insulators," *IEEE Trans. Dielectr. Electr. Insul.*, vol. 17, no. 2, pp. 375–383, Apr. 2010.

[42] L. Cheng, L. Wang, Z. Guan, and F. Zhang, "Aging characterization and lifespan prediction of silicone rubber material utilized for composite insulators in areas of atypical warmth and humidity," *IEEE Trans. Dielectr. Electr. Insul.*, vol. 23, no. 6, pp. 3547–3555, Dec. 2016.

[43] C. Yuan, C. Xie, L. Li, X. Xu, and S. M. Gubanski, "Surface potential decay on material samples taken from in-service aged HVDC silicone rubber composite insulators," *IEEE Trans. Dielectr. Electr. Insul.*, vol. 24, no. 1, pp. 592–600, Feb. 2017.

[44] N. Mavrikakis, K. Siderakis, P. Mikropoulos, and N. Katsarakis, "Condition assessment of a field-aged 150 kV HTV SIR suspension insulator following flashover," in *Proc. ISH 19th Int. Symp. High Voltage Eng.*, Pilsen, Czech Republic, 2015, pp. 1–6.

[45] N. Mavrikakis, K. Siderakis, and P. N. Mikropoulos, "Laboratory investigation on hydrophobicity and tracking performance of field aged composite insulators," in *Proc. 49th Int. Universities Power Eng. Conf. (UPEC)*, Sep. 2014, pp. 1–6.

[46] H. Khan, A. Mahmood, I. Ullah, M. Amin, and M. T. Nazir, "Hydrophobic, dielectric and water immersion performance of 9000 h multi-stresses aged silicone rubber composites for high voltage outdoor insulation," *Eng. Failure Anal.*, vol. 122, Apr. 2021, Art. no. 105223.

[47] M. Akbari and A. A. Shayegani-Akmal, "Experimental investigation on the accelerated aging of silicone rubber insulators based on thermal stress," *Int. J. Electr. Power Energy Syst.*, vol. 149, Jul. 2023, Art. no. 109049.

[48] *Artificial Pollution Tests on High Voltage Insulators to be Used on Ac Systems*, 2nd ed., IEC, Geneva, Switzerland, 1991.

[49] *Guidance on the Measurement of Wettability of Insulator Surfaces*, T. IEC, Geneva, Switzerland, 2003.

[50] M. Akbar, R. Ullah, and S. Alam, "Aging of silicone rubber-based composite insulators under multi-stressed conditions: An overview," *Mater. Res. Exp.*, vol. 6, no. 10, Sep. 2019, Art. no. 102003.

[51] V. V. Rao, "Assessment of insulation failure of field aged 11 kV polymeric insulators of marine environment with characterizations technique," *J. Failure Anal. Prevention*, vol. 23, no. 5, pp. 1932–1939, Oct. 2023.

[52] X. Qiao, Y. Ming, K. Xu, N. Yi, and R. Sundararajan, "Aging of polymeric insulators under various conditions and environments: Another look," *Energies*, vol. 15, no. 23, p. 8809, Nov. 2022.

[53] X. Peng, H. Lin, R. Wang, Z. Wang, and P. Fang, "Review on aging mechanism and service life prediction of silicone rubber composite insulator," *High Voltage Apparel*, vol. 54, pp. 1–8, Jan. 2018.
[54] T. Imakoma, Y. Suzuki, O. Fujii, and I. Nakajima, "Degradation of silicone rubber housing by ultraviolet radiation," in *Proc. 4th Int. Conf. Properties Appl. Dielectr. Mater. (ICPADM)*, 1994, pp. 306–308.
[55] S. N. Haya, A. A. Jaelani, and L. S. Lumba, "Accelerated aging study on silicone rubber insulator with contaminant level and fog conductivity variations," in *Proc. 3rd Int. Conf. High Voltage Eng. Power Syst. (ICHVEPS)*, Oct. 2021, pp. 091–095.
[56] R. Saldivar-Guerrero, R. Hernández-Corona, F. A. Lopez-Gonzalez, L. Rejón-García, and V. Romero-Baizabal, "Application of unusual techniques for characterizing ageing on polymeric electrical insulation," *Electr. Power Syst. Res.*, vol. 117, pp. 202–209, Dec. 2014.
[57] *High-Voltage Test Techniques—Part 1: General Definitions Test Requirements*, HVT Techn., Geneva, Switzerland, 2010.
[58] W. Wang, H. Lu, C. Li, Y. Deng, L. Lan, X. Wen, B. Luo, and W. Xiao, "Study on the relationship between the characteristics of water droplets on the shed of composite insulators and the pollution flashover voltage," *Energy Rep.*, vol. 8, pp. 1071–1077, Aug. 2022.
[59] A. Aman, M. M. Yaacob, M. A. Alsaedi, and K. A. Ibrahim, "Polymeric composite based on waste material for high voltage outdoor application," *Int. J. Electr. Power Energy Syst.*, vol. 45, no. 1, pp. 346–352, Feb. 2013.
[60] E. M. Savadkoohi, M. Mirzaie, S. Seyyedbarzegar, M. Mohammadi, M. Khodsuz, M. G. Pashakolae, and M. B. Ghadikolaei, "Experimental investigation on composite insulators AC flashover performance with fan-shaped non-uniform pollution under electro-thermal stress," *Int. J. Electr. Power Energy Syst.*, vol. 121, Oct. 2020, Art. no. 106142.
[61] M. Ramesh, L. Cui, Y. Shtessel, and R. Gorur, "Failure studies of polymeric insulating materials using sliding mode observer," *Int. J. Electr. Power Energy Syst.*, vol. 126, Mar. 2021, Art. no. 106539.
[62] F. Aouabed, A. Bayadi, A. E. Rahmani, and R. Boudissa, "Finite element modelling of electric field and voltage distribution on a silicone insulating surface covered with water droplets," *IEEE Trans. Dielectr. Electr. Insul.*, vol. 25, no. 2, pp. 413–420, Apr. 2018.
[63] T. Takuma and T. Kawamoto, "Field intensification near various points of contact with a zero contact angle between a solid dielectric and an electrode," *IEEE Trans. Power App. Syst.*, vol. PAS-103, no. 9, pp. 2486–2494, Sep. 1984.
[64] T. Takuma, "Field behaviour at a triple junction in composite dielectric arrangements," *IEEE Trans. Electr. Insul.*, vol. 26, no. 3, pp. 500–509, Jun. 1991.
[65] T. Takuma and B. Techaumnat, *Electric Fields in Composite Dielectrics and Their Applications*. Cham, Switzerland: Springer, 2010.
[66] M. Bouhaouche, A. Mekhaldi, and M. Teguar, "Improvement of electric field distribution by integrating composite insulators in a 400 kV AC double circuit line in Algeria," *IEEE Trans. Dielectr. Electr. Insul.*, vol. 24, no. 6, pp. 3549–3558, Dec. 2017.
[67] Y. Shi, G. Xie, Q. Wang, X. Li, X. Yang, P. Liu, and Z. Peng, "Simulation analysis and calculation of electric field distribution characteristics of UHV wall bushing," *Energy Rep.*, vol. 7, pp. 110–117, Nov. 2021.
[68] M. M. Ispirli, B. Oral, and Ö. Kalenderli, "Electric field analysis of 66 kV and 110 kV SiR insulators under combined AC–DC voltages," *Energy Rep.*, vol. 8, pp. 361–368, Apr. 2022.
[69] Z. Zhang, G. Pang, M. Lu, C. Gao, and X. Jiang, "Research on silicone rubber sheds of decay-like fractured composite insulators based on hardness, hydrophobicity, NMR, and FTIR," *Polymers*, vol. 14, no. 16, p. 3424, Aug. 2022.
[70] S. M. Rowland, Y. Xiong, J. Robertson, and S. Hoffmann, "Aging of silicone rubber composite insulators on 400 kV transmission lines," *IEEE Trans. Dielectr. Electr. Insul.*, vol. 14, no. 1, pp. 130–136, Feb. 2007.

MANSOOR ASIF received the B.E. degree from the National University of Sciences and Technology (NUST), Islamabad, Pakistan, in 2013, the M.S. degree from North China Electric Power University, Beijing, China, in 2015, and the Ph.D. degree from Hanyang University, Ansan, South Korea, in 2020. He is currently associated with the Applied Research Center for Metrology Standards and Testing, King Fahad University of Petroleum and Minerals (KFUPM), Saudi Arabia. His research interests include numerical analysis of high voltage assets, condition monitoring and diagnostics (CMD) of high voltage equipment, and machine learning applications in CMD.

KHALED AL-SOUFI was born in Jordan, in 1957. He received the B.Sc. degree in electrical engineering from King Abdulaziz University, Saudi Arabia, in 1981, and the M.Sc. degree in electrical engineering from the King Fahd University of Petroleum and Minerals (KFUPM), Dhahran, Saudi Arabia, in 1985. He is currently a Research Engineer III with the Applied Research Center for Metrology Standards and Testing, Research and Innovation, KFUPM, where he is actively participating in teaching, and managing various client and internally funded research projects. His research interests include high voltage insulators, power systems analysis and studies, and supervising the high voltage laboratory of KFUPM.

UMER AMIR KHAN received the B.E. degree from the National University of Sciences and Technology (NUST), Islamabad, Pakistan, in 2006, and the M.S. and Ph.D. degrees from Hanyang University, Ansan, South Korea, in 2011 and 2016, respectively. He is currently associated with the Department of Electrical Engineering, King Fahad University of Petroleum and Minerals (KFUPM), Saudi Arabia. His research interests include condition monitoring and diagnostics (CMD) of high voltage equipment, machine learning applications in CMD and renewable energy integration, high voltage engineering, protection systems for HVDC systems, and smart grids.

LUAI M. ALHEMS received the Ph.D. degree from Texas A&M University, College Station, TX, USA, in 2002. He is currently a Professor with the Department of Mechanical Engineering, King Fahd University of Petroleum and Minerals (KFUPM), Dhahran, Saudi Arabia. He is also the Director of the Applied Research Center for Metrology, Standards, and Testing (ARC-MST) Research and Innovation. Regional authorities have recognized him for his research work. He has authored or coauthored more than 180 journal articles and patents. His research interests include gas turbines, energy systems, failure analysis, wind energy, and energy conservation.